LUT UNIVERSITY
LUT School of Energy Systems
LUT Mechanical Engineering

Ilkka Hyvönen

FATIGUE STRENGTH OF A BOLT UNDER PULSATING COMPRESSIVE STRESS

Examiners: Professor Timo Björk
M. Sc. Mehrdad Javadi

TIIVISTELMÄ

LUT University
LUT School of Energy Systems
LUT Kone

Ilkka Hyvönen

Pultin väsymislujuus tykyttävässä puristuskuormituksessa

Diplomityö

2021

62 sivua, 36 kuvaa, 30 taulukkoa, 4 liitettä

Tarkastajat: Professori Timo Björk
DI Mehrdad Javadi

Hakusanat: väsymislujuus, ruuvikierre, kitkaväsyminen, puristusjännitys, esikiristys

Tämän tutkimuksen tavoitteena on perehtyä tykyttävässä puristuskuormituksessa olevan pultin väsymislujuuteen vaikuttaviin päätekijöihin, sekä selvittää pultin esikiristysvoiman kasvattamisen mahdollisia etuja ja haittoja.

Kierreliitoksen lovenmuotolukuja tutkitaan epäsymmetrisen kuormituksen alaisena ja kahdella erilaisella materiaalimallilla. Pultin suurin muotoluku ja reaktiovoima ovat ensimmäisellä kontaktissa olevalla kierteellä, mutta suurimmat leikkausjännitykset ovat viimeisellä kontaktissa olevalla kierteellä. Pultin väsymislujuutta on mahdollista parantaa kartiomaisella profiililla, jolloin kuorma jakautuu tasaisemmin eri kierteille.

Esikiristysvoiman kasvattaminen ei automaattisesti alenna pultin jännitysamplitudia, koska tämä on riippuvaista ruuviliitoksen rakenteesta ja lisävoimakertoimesta. Ruuvin varren väsymisvaurio ei ole odotettavissa, ellei taivutusjännityskomponentti ole riittävän suuri aiheuttamaan varteen vetojännitystilan. Puristuskuormitteisen ruuvin väsymisvaurio tapahtuu todennäköisimmin ruuvin kierteiden tai kannan leikkaantumisena.

ABSTRACT

LUT-Yliopisto
LUT School of Energy Systems
LUT Mechanical Engineering

Ilkka Hyvönen

Fatigue strength of a bolt under pulsating compressive stress

Master's thesis

2021

62 pages, 36 figures, 30 tables, 4 appendices

Examiners: Professor Timo Björk
M. Sc. Mehrdad Javadi

Keywords: fatigue strength, bolt thread, fretting fatigue, compressive stress, bolt preload

This research aims to find out the main factors about fatigue strength of a bolt that is under pulsating compressive stress and to analyze the potential benefits and disadvantages of increasing the bolt preload.

The stress distribution of threads is studied with the finite element method. The highest stress concentration factor and reaction forces of the bolt are found in the first contacting thread, but the highest shear stress values are in the last contacting thread. The fatigue strength of the bolt can be improved by tapered threads, which distribute the load more evenly between threads.

Increased bolt preload does not automatically reduce the stress amplitude, but it is dependent on the bolt joint configuration and bolt load ratio of the joint. Fatigue damage of the shank is not expected if the bending stress component is not high enough to cause a tensile state to the shank. Fatigue failure of a compression-loaded bolt is most likely going to occur by shearing of threads or by shearing of the bolt head.

ACKNOWLEDGEMENTS

Fundamental work of this thesis was done for Sandvik in Australia during the year 2020, and writing work was finalized in Finland in 2021. I appreciate that I have had the possibility to work in a global environment with people from all over the world, which has been an enriching experience.

I would like to thank my examiners M. Sc. Mehrdad Javadi and Professor Timo Björk, for their support with the thesis. I would also like to thank Bruce Knowles for the development work of the test bench that was used in the testing of bolted joints.

Ilkka Hyvönen

Turku 24.5.2021

TABLE OF CONTENTS

LIST OF SYMBOLS AND ABBREVIATIONS

Symbols

a	Material constant [mm]
A_3	Cross-sectional area of bolt shank [mm^2]
A_{red}	Cross-sectional area of the reduced cylinder [mm^2]
b	Fatigue strength exponent
β_1	Flank angle [deg]
β_2	Flank angle [deg]
c	Fatigue ductility exponent
C	End condition constant
D	Basic major diameter of internal thread [mm]
d	Basic minor diameter of external thread [mm]
D_1	Basic minor diameter of internal thread [mm]
d_1	Basic minor diameter of external thread [mm]
D_2	Basic pitch diameter of internal thread [mm]
d_2	Basic pitch diameter of external thread [mm]
D_{red}	Outer diameter of the reduced cylinder [mm]
d_K	Diameter of bearing surface of the bolt [mm]
D_B	Hole diameter [mm]
D_A	Outer diameter [mm]
D_{km}	Average diameter of bearing surface of the bolt [mm]
Δ_{SV}	Bolt extension [mm]
Δ_{PV}	Compression of the joint parts [mm]
E	Young’s modulus [GPa]
E_t	Tangent modulus [GPa]
E_P	Elastic modulus of compressed parts [GPa]
e	Nominal strain
ε	Strain
ε_e	Elastic strain

ε_p	Plastic strain
ε_{root}	Total strain at root of the thread
ε_f'	Fatigue ductility coefficient
F_A	External load [N]
F_L	External force, left-hand side bearing face [N]
F_M	Axial force of the bolt during the torquing [N]
F_n	Normal force [N]
F_{PA}	Reduction in clamping force [N]
F_R	External force, right-hand side bearing face [N]
F_S	Bolt load [N]
F_{SA}	Bolt load increase by the external load [N]
F_V	Bolt preload [N]
f_{Ln}	Reaction force of *n*th thread of left-hand side of the bolt [N]
f_{Rn}	Reaction force of *n*th thread of right-hand side of the bolt [N]
γ	Lead angle [deg]
H	Height of fundamental triangle [mm]
I	Second moment of area [mm^4]
K_t	Stress concentration factor
K_f	Fatigue notch factor
K_ε	Strain concentration factor
K'	Cyclic strength coefficient [MPa]
K_σ	Stress concentration factor
K_{bLn}	SCF of *n*th thread of left-hand side of the bolt
K_{bRn}	SCF of *n*th thread of right-hand side of the bolt
K_{nLn}	SCF of *n*th thread of left-hand side of the nut
K_{nRn}	SCF of *n*th thread of right-hand side of the nut
kS	Combined spring constant of bolt and nut *[N/mm]*
k_{GM}	Combined spring constant of nut and section of bolt that is within the nut [N/mm]
k_K	Spring constant of the bolt head [N/mm]
k_i	Spring constant of section *i* of the bolt [N/mm]
L	Length [mm]

L_e	Load eccentricity [mm]
L_L	Moment arm of the external force, left-hand side [mm]
L_R	Moment arm of the external force, right-hand side [mm]
L_1	Average distance between load-bearing faces [mm]
l_K	Combined thickness of the joint parts [mm]
k_P	Spring constant of compressed sections in joint [mm]
M_A	Bolt tightening torque [N m]
M_G	Frictional moment of bearing surface of the bolt [N m]
M_K	Frictional moment of the thread [N m]
N	Number of load cycles
n	External load point multiplier
n'	Cyclic strain hardening component
P	Pitch [mm]
ρ	Notch radius [mm]
q	Notch sensitivity factor
P_{cr}	Critical load [N]
Q	Frictional force [N]
σ_{max}	Maximum stress [MPa]
σ_{min}	Minimum stress [MPa]
σ	Stress [MPa]
σ_m	Mean stress [MPa]
σ_a	Stress amplitude [MPa]
σ_r	Stress range [MPa]
σ_1	Maximum principal stress [MPa]
σ_2	Minimum principal stress [MPa]
$\sigma_{VonMises}$	Von Mises stress [MPa]
σ_b	Bending stress component [MPa]
$\Delta\sigma$	Stress range [MPa]
σ_0	Nominal stress [MPa]
σ_f'	Fatigue strength coefficient
R_m	Ultimate tensile strength [MPa]

R_e	Yield strength [MPa]
R_{ec}	Compressive yield strength [MPa]
R	Stress ratio
S	Stress amplitude [MPa]
τ_{max}	Maximum shear stress [MPa]
t_1	Thickness parameter [mm]
Φ	Bolt load ratio
μ	Friction coefficient
μ_G	Friction coefficient of the thread
μ_K	Friction coefficient of bearing surface of bolt
ν	Poisson's ratio
x	Dimensionless bolt joint type variable

Abbreviations

LHD	Load Haul Dump
SCF	Stress Concentration Factor
UNC	Unified National Coarse thread
UNR	Unified National Thread Series with external thread controlled root radius

1 INTRODUCTION

The reliability of dynamically loaded bolted joints is, in many cases challenging engineering problem because of several variables that affect the fatigue phenomenon. Load history may be unknown, friction coefficients have variation, the vibration of parts, human errors during the assembly phase of the components, to name a few. Oversized bolts increase manufacturing costs and may also have other adverse effects on the performance of the product due to higher rigidity, larger weight, and size.

1.1 Background of the work

The reason for the research work is to study possibilities to improve the reliability of compression loaded bolt joint that is used in underground mining applications. Work is done for Sandvik AB, which has been the leading manufacturer of underground load, haul, dump (LHD) machines in the world. The public version of the thesis excludes the experimental portion and details about bolted joint of the end application and focuses on inspecting the fatigue strength of the bolt and the nut.

1.2 Research problem

Fatigue strength of the bolted joint is typically increased by using as high preload as possible so that the stress amplitude of the bolt under external load is minimized. This generalization does not necessarily apply to unconventional bolted joints where the bolt is constantly under compressive load and if the spring constant of clamped parts is less than the spring constant of the bolt.

Finding out the optimal preload for a bolt that is under pulsating compressive stress requires an understanding of the characteristics of the bolt joint. The relationship between fatigue strength to stress amplitude, mean stress, stress concentration factor of threads, and fretting fatigue phenomenon needs to be studied. Optimal fatigue strength of the bolted joint under specific constant stress amplitude does not necessarily lead to optimal reliability of the bolted joint in actual end application if reserve capacity to random impact loads is reduced due the fatigue load optimization.

1.3 Objectives

The objective of the research is to identify the most important factors of compression-loaded bolted joints. Results of the study are utilized to enhance the reliability of existing products and with new product development.

1.3.1 Research questions

The primary research question: What is the fatigue strength of compression-loaded 1” unified national coarse threaded (UNC) bolted joint, and what are the most significant factors that contribute to the fatigue strength of such joint.

The second research question is whether the fatigue strength of compression-loaded bolted joint could be improved by changing the thread geometry of the bolt.

1.3.2 Hypotheses of the study

The hypotheses of the study are following. Currently used bolt tightening torque of 1” UNC threaded bolt is not optimized for fatigue life in terms of bolt preload. Typical torque values used with end application are based on using bolt tightening torques that can be achieved with usual torque wrenches and bolt preload could be increased by changing the thread pitch.

The second hypothesis is that the fatigue life of the bolted joint could be improved by using a thread geometry that distributes stress more evenly to several threads.

1.4 Research methods

The first phase of the work investigates earlier research and theory about factors relevant to fatigue strength of threaded joints and parts under compressive stress. This includes an examination of bolted joint diagrams, Goodman-Smith diagram, crack propagation under compressive load, and fretting fatigue phenomenon.

The second phase of the work is to perform two-dimensional FEA simulations to bolts with eccentric loading using different thread geometries, bolt load values and to examine results by applying strain-life analysis to estimate the fatigue strength of the bolt.

1.5 Scope

This research is focused on compression-loaded bolts where bolt preload is compressive and external load that is applied to the joint increases compressive stress levels of the bolt. Most research and theory about bolted joints cover tension-loaded bolts. Compression-loaded bolted joint will add some design aspects that are not present with tension-loaded bolts, such as buckling of the bolt, for example.

Different material options or thread manufacturing methods for the bolt are left out of the scope of this research work. Fatigue life calculation of threads using fracture mechanics is not included in this research due to the broadness of the work. Understanding the basic characteristics of the bolted joint is a requirement for more accurate fatigue analysis. The focus of the study is on the threaded joint. Strength analysis of the bolt head is not included in the work.

Only a single bolt size is being studied in this research. This research works as a baseline for possible examination and testing of different types of threads in the future for further reliability improvements of products.

2 FATIGUE STRENGTH OF BOLTED JOINTS

Bolted joints are commonly used in machine design, among other things, due to their ease of assembly that usually does not require specialized skills, moderate price, and good availability of components. Bolted joints can be used in locations where high dimensional accuracy or the ability to disassemble the parts is required.

2.1 Reliability of bolted joints

The reliability of a bolted joint under static load is good, but under dynamic load conditions, there are several factors that can result in compromised reliability of the joint. Bolted joints can also be designed to be the weakest link in the structure on purpose to avoid a more harmful type of failure of some other component.

2.1.1 Thread profile

Fastener bolts typically use a thread profile that is based on metric ISO 68-1 or imperial ASME B1.1 UNS standards. Both these standards share a similar parallel V-shaped 60° thread profile, but diameters and pitch distances between the two are different. Coarse threads have a larger pitch distance, and they are more commonly used than fine threads.

Manufacturing of the most common thread profiles can be made by machining or by cold forming. When threads are manufactured by cold forming, the rolling process creates strain hardening and residual stresses to the material, which can improve the fatigue strength of the threads. (Kim et al. 2007, p. 46).

There are several different types of thread profiles that have been developed for specific applications, such as trapezoidal threads that are used for creating motion or tapered threads that create a sealing effect by compressing against each other when the joint is tightened. Cross-sections and different parts of commonly used thread geometry are illustrated in figures 1 and 2. Abbreviations and terminology of thread profile are described in tables 1 and 2.

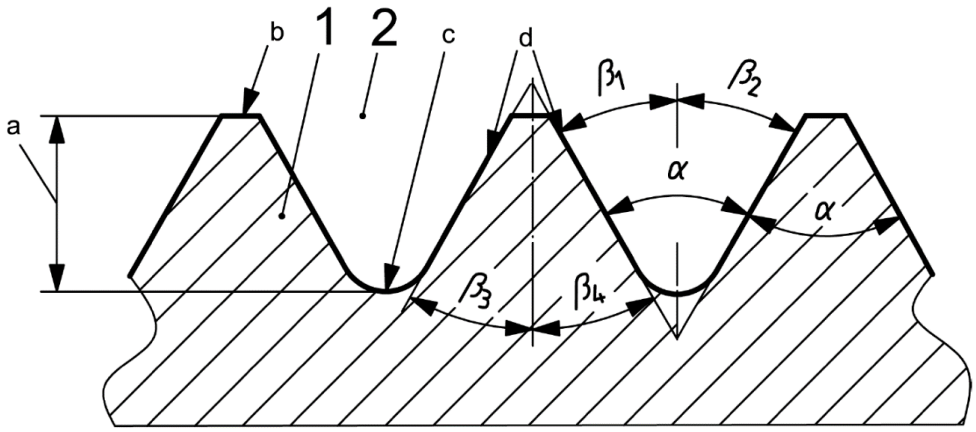

Figure 1. Sections and dimensions of thread profile (SFS-ISO 5408, 2010, p. 19).

Table 1. Terminology of screw threads (SFS-ISO 5408, 2010, p. 19).

1	Ridge	b	Crest
2	Groove	c	Root
a	Thread height	d	Flank

Thread is unsymmetrical when flank angles β_1 and β_2 have different values. The root of the thread groove typically has a fillet that impacts the notch effect of the thread.

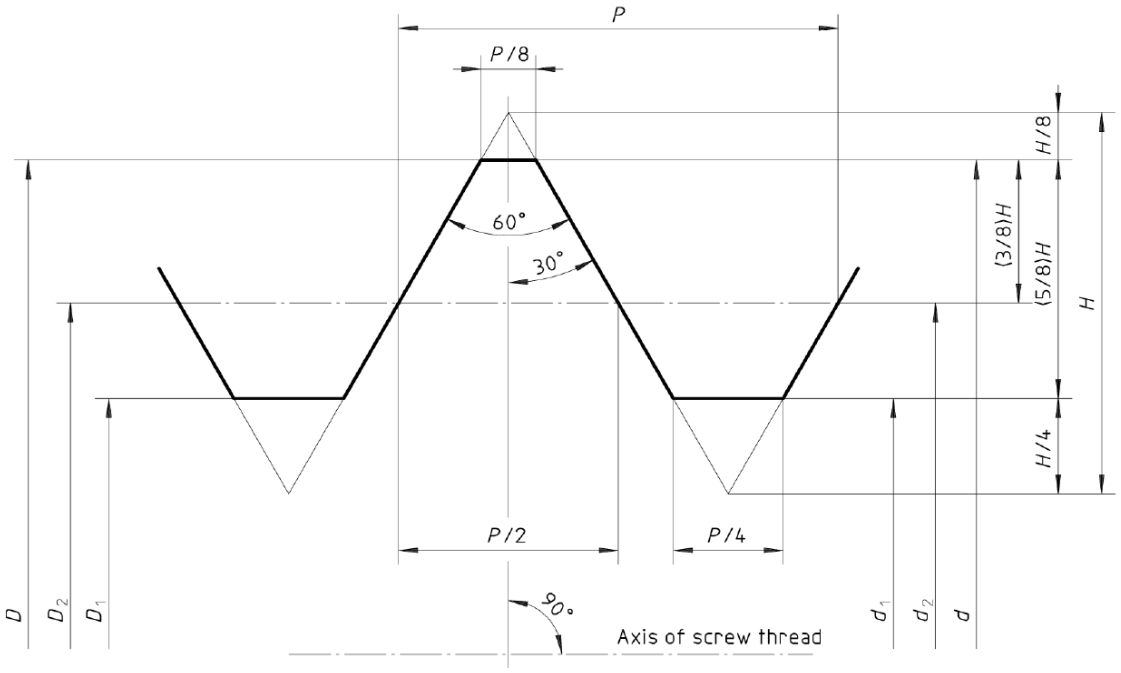

Figure 2. Profile of metric ISO thread (SFS-ISO 68-1, 2010, p. 7).

Table 2. Abbreviations of figure 2. Metric ISO thread (SFS-ISO 68-1, 2010, p. 7).

D	Basic major diameter of internal thread (nominal diameter)
d	Basic major diameter of external thread (nominal diameter)
D_2	Basic pitch diameter of internal thread
d_2	Basic pitch diameter of external thread
D_1	Basic minor diameter of internal thread
d_1	Basic minor diameter of external thread
H	Height of fundamental triangle
P	Pitch

Opposite flanks form the fundamental triangle of the thread, which has a height of H. In the metric ISO thread fundamental triangle is equiangular.

Lead angle, thread pitch and pitch diameter are illustrated in figure 3.

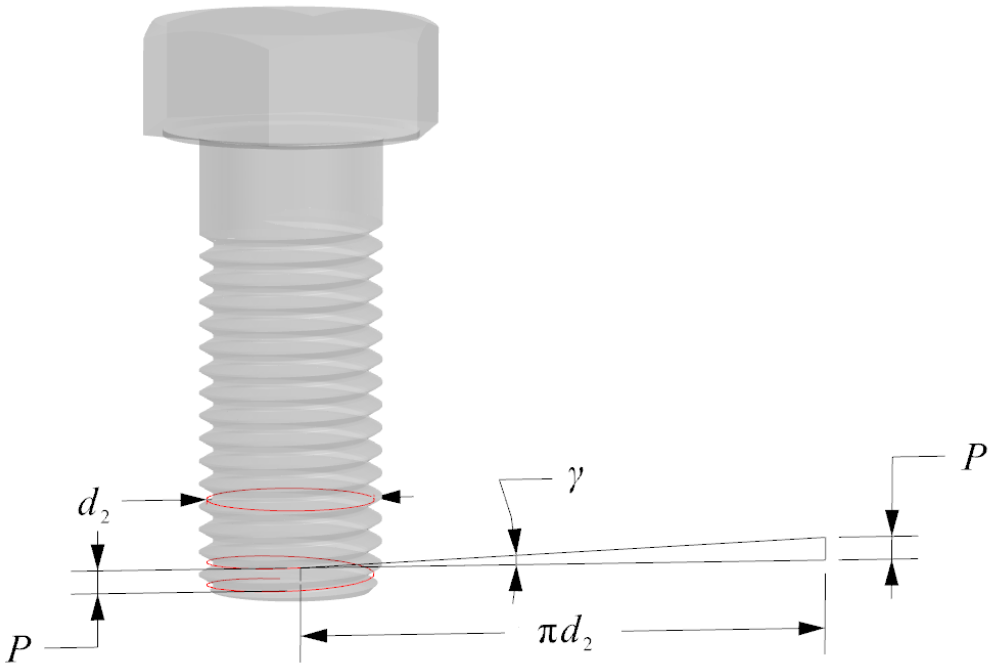

Figure 3. Lead angle γ of thread.

Lead angle γ depends on the thread pitch P and diameter. The lead angle of the thread is calculated by the following formula (Airila. et al. Koneenosien suunnittelu, 2010, p. 162).

$$\gamma = \arctan\frac{P}{\pi d_2} \tag{1}$$

Where d_2 is the pitch diameter of the thread.

2.1.2 Bolted joint diagram of tension loaded bolt joint

Bolt will be subjected to forces that are dependant on external load, tightening torque, bolt pretension, and structure of the bolt joint. In a typical tension-loaded bolt joint, the bolt stretches, and clamped parts compress in the area that is between the bolt head and nut. When external load F_A is applied to the joint, the tension of the bolt increases while compression stress of clamped parts between the bolt head and nut reduces. Figure 4 shows cross-section of tension loaded bolted joint with compressed sections of clamped parts.

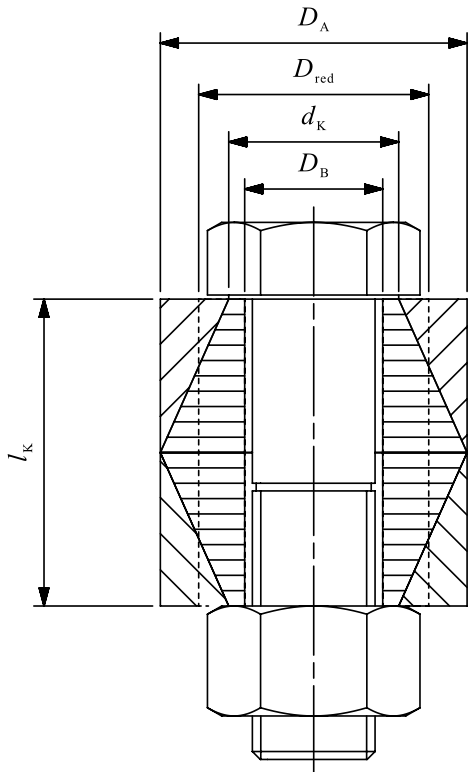

Figure 4. Conical sections express compressed areas in the bolt joint.

Combined spring constant k_S of a bolt with nut can be determined by adding spring constants of the nut and sections the of the bolt in series (Airila et al. 2010, p. 199).

$$k_S = \left(\frac{1}{k_{GM}} + \frac{1}{k_K} + \sum_{1}^{n} \frac{1}{k_i} \right)^{-1} \quad (2)$$

Table 3. Abbreviations of equation 2.

k_S	Combined spring constant of bolt and nut
k_{GM}	Combined spring constant of nut and section of the bolt that is within the nut
k_K	Spring constant of the bolt head
k_i	Spring constant of section *i* of the bolt

The spring constant of compressed sections in the joint can be calculated by using reduced cylinder area A_{red}, which has an outer diameter of D_{red} (figure 4). Reduced cylinder area can be calculated by using the following formula in joints where $d_k \leq D_A \leq d_k + l_k$ (Airila. et al. 2010, p. 200).

$$A_{\mathrm{red}} = \frac{\pi}{4}(d_{\mathrm{K}}^2 - D_{\mathrm{B}}^2) + \frac{\pi}{8} d_{\mathrm{K}}(D_A - d_{\mathrm{K}})(x+2)x \quad (3)$$

When bolt joint type includes a nut, dimensionless variable *x* is calculated by the following equation (Airila et al. 2010, p. 200).

$$x = \sqrt[3]{\frac{l_{\mathrm{K}} d_{\mathrm{K}}}{D_{\mathrm{A}}^2}} \quad (4)$$

Table 4. Abbreviations of equations 3 and 4.

A_{red}	Cross sectional area of reduced cylinder
D_{red}	Outer diameter of reduced cylinder
d_{K}	Diameter of bearing surface of the bolt
D_{B}	Hole diameter
D_{A}	Outer diameter
x	Dimensionless bolt joint type variable
l_{K}	Combined thickness of the joint parts

Spring constant k_{P} of compressed sections in joint is calculated with the following equation:

$$k_{\mathrm{P}} = \frac{A_{\mathrm{red}} E_{\mathrm{P}}}{l_{\mathrm{K}}} \quad (5)$$

Table 5. Abbreviations of equation 5.

k_{P}	Spring constant of compressed sections in joint
E_{P}	Elastic modulus of compressed parts

Line *s*, shown in figure 5, represents the force-displacement relationship of the bolt, and line *p* is the force-displacement curve of clamped parts. Slopes of curves are determined by spring constants k_S and k_P. In figure 5, the slope of clamped parts is steeper than the slope of the bolt. When external load F_A is applied to the joint, the compressive force of clamped parts reduces by F_{PA}, and tension of the bolt increases by F_{SA}. This means that the stress amplitude of the bolt is not dependent only on the amount of external load. Stress amplitude also depends on the bolt pretension force F_V and the stiffness ratio between bolt and clamped parts. Abbreviations of used in bolted diagram are described in table 6.

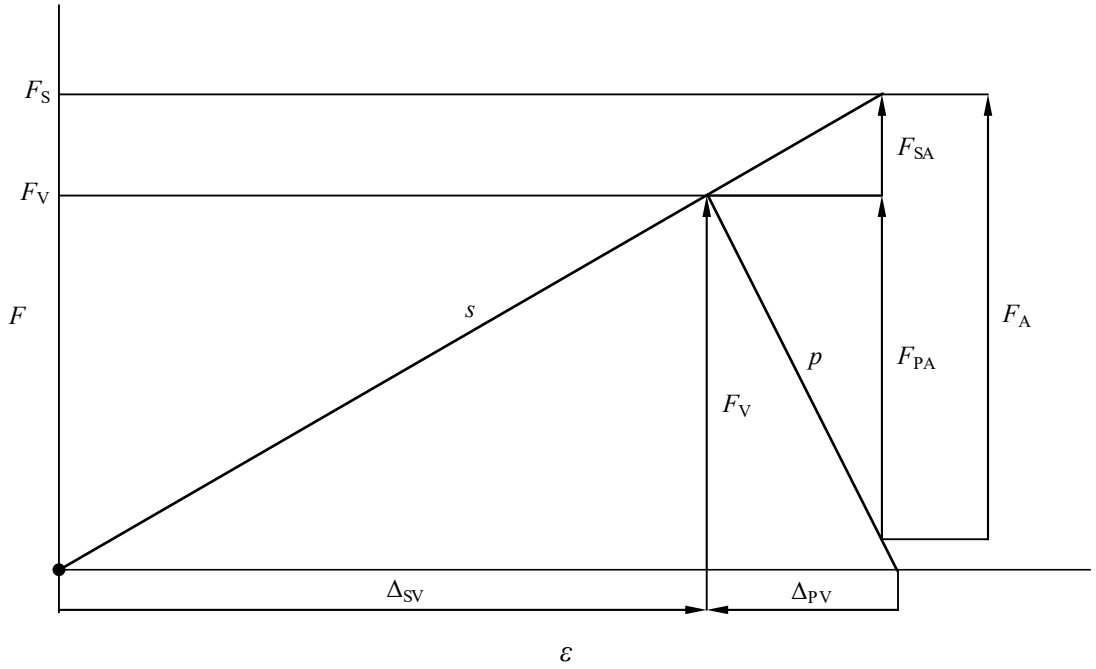

Figure 5. Bolted joint diagram. Spring constant $k_S < k_P$.

Table 6. Abbreviations of figure 5.

F_S	Bolt load
F_V	Bolt preload
F_A	External load
F_{SA}	Bolt load increase by the external load
F_{PA}	Reduction in clamping force
Δ_{SV}	Bolt extension
Δ_{PV}	Compression of the clamped parts

The bolted joint diagram in figure 6 represents bolted joint where the spring constant of the bolt is higher than the spring constant of clamped parts. When external load F_A is applied to the joint, only a small portion of the force is reduced by decompression of clamped parts F_{PA}, and the majority of the force increases bolt load F_S by the amount of F_{SA}. This type of bolted joint is sensitive to an excess amount of bolt pretension because most of the external load F_A transfers to bolt load increase F_{SA}. Oversized diameter and short bolt length lead to rigid bolt with high spring constant, which is not optimal for the bolted joint structure.

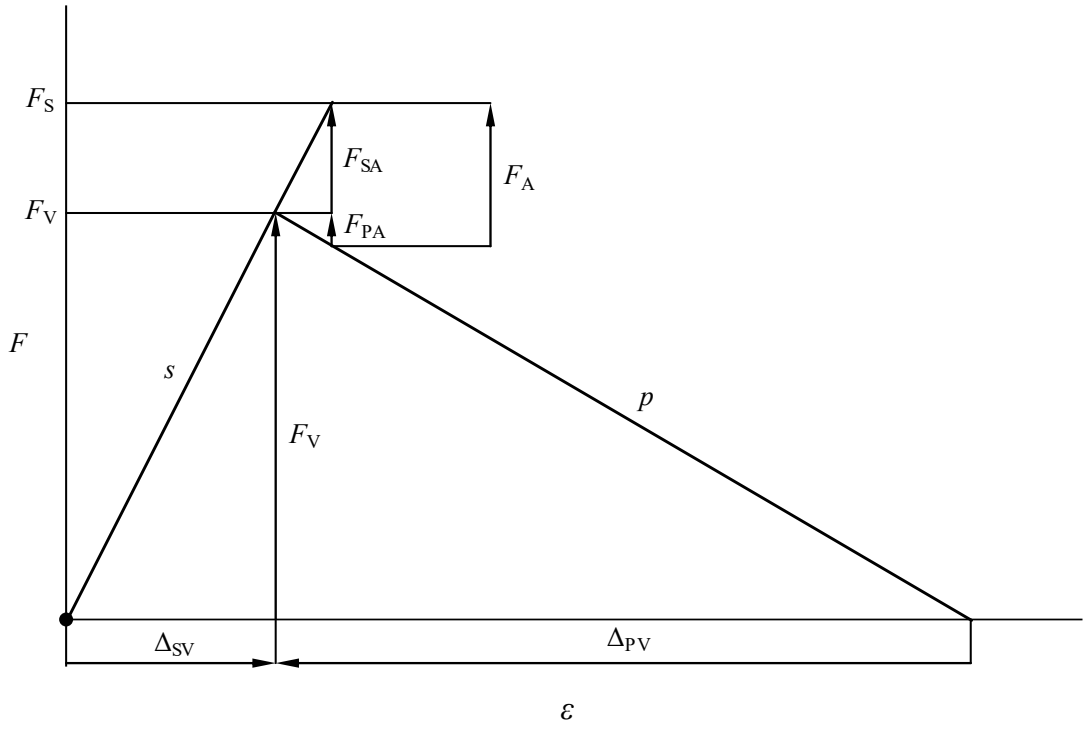

Figure 6. Bolted joint diagram. Spring constant $k_S > k_P$.

2.1.3 Bolted joint diagram of compression loaded bolt joint

Bolted joint of this study differs from the typical bolted joint in the sense that bolt preload is introduced as a compressive force to the bolt and that external loads applied to the bolted joint transfer into increasing compressive stress levels of the bolt.

Bolt preload F_V causes compressive stress to the bolt. External force F_A increases compressive stress and adds bending load to the shank section of the bolt. Bending moment increases shear forces of threads and elevates stress levels at thread roots.

Using reduced cylinder area A_{red} as per equation (3) for modeling the spring constant of clamped parts is not suitable for this bolted joint due to the structural differences and how external load is applied eccentrically to the joint. The structure of the bolted joint can be such that it creates force multiplication to the bolt. This force multiplication is described as bolt load ratio.

Generation of bolted joint diagram requires determination of spring constants of the bolt and clamped parts. The spring constant of the bolt is k_S, which consists of spring constants k_{GM} (thread engagement area of bolt and nut), k_2 (shank), and k_K (crown). The effective spring constant of clamped parts is k_{Pe}.

Bolted joint diagram of compressively loaded eccentric bolted joint illustrated in figure 7 differs from the cylindrical tension-loaded bolted joint diagram in a way that strain and force values are presented at negative ranges, and that bolt load reduction from the release of clamped parts F_{PA} is not present in the system. Applied external load F_A to the joint is added on top of bolt preload F_V with bolt load multiplication that varies depending on the load and other conditions. This type of bolted joint diagram does not generalize all compression-loaded bolted joints. The relationship between bolt load and the externally applied force is case-specific.

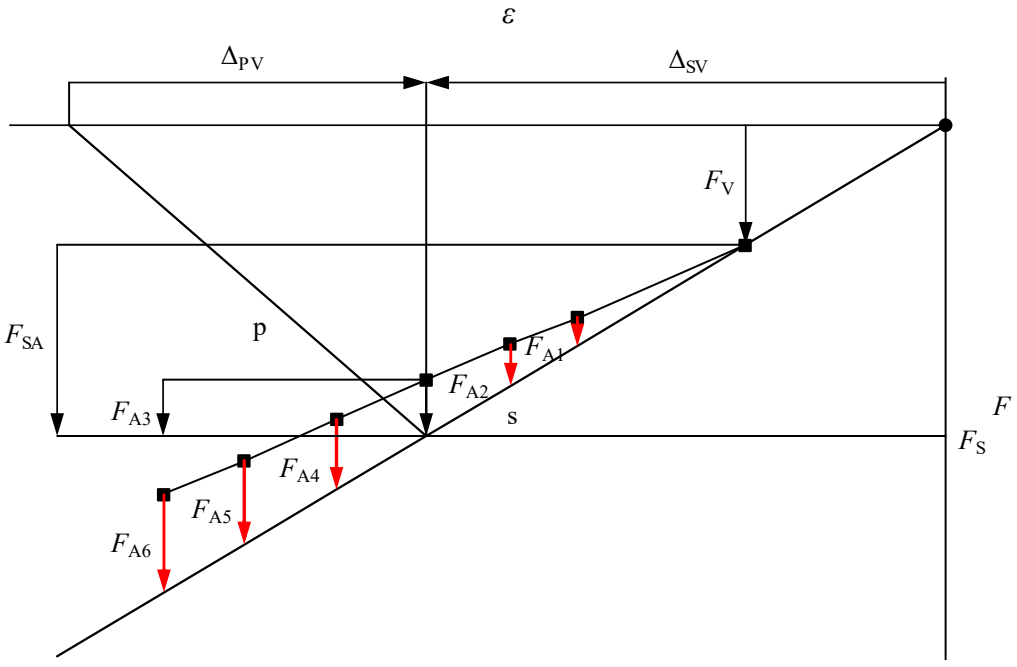

Figure 7. Bolted joint diagram compressive loaded eccentric bolted joint.

Bolt preload F_V adds compressive force to bolt, causing negative strain -ε. Clamped parts are under tension after bolt preload has been added, causing positive strain ε to clamped parts. When external load F_A is applied to the structure, compressive stress levels of bolt increase and tensile stresses on clamped parts grow.

The bolted joint diagram in figure 7 is created by calculated spring constants and measured bolt load values. Varying external loads $F_{A1}…F_{A6}$ results in high bolt load increase F_{SA} values due to the bolt load multiplication of the structure.

2.1.4 Bolt preload

Good reliability of bolted joint requires high enough bolt preload $F_{V,}$ so that the joint does not unfasten by itself due to vibrations or external load. Another beneficial effect of bolt preload is the reduction of bolt load increase F_{SA} when an external load is applied to the joint. However, too high bolt preload may lead to excessively high stress levels and failure of the bolt.

Required bolt tightening torque to achieve desired bolt preload is determined by the combination of a frictional moment of the thread and a frictional moment of the bearing surface of the bolt. Bolt tightening torque is calculated by the following equation (Airila. et al. 2010, p. 231).

$$M_A = M_G + M_K = \frac{1}{2} F_M \left(1{,}155 \mu_G d_2 + \mu_K D_{km} + \frac{P}{\pi}\right) \quad (6)$$

Table 7. Abbreviations of equation 6.

M_A	Bolt tightening torque
M_G	Frictional moment of bearing surface of the bolt
M_K	Frictional moment of the thread
F_M	Axial force of the bolt during the torquing
μ_G	Friction coefficient of the thread
μ_K	Friction coefficient of bearing surface of the bolt
D_{km}	Average diameter of bearing surface of the bolt

Average diameter D_{km} is the mean of hole diameter D_B and diameter of bearing surface of the bolt d_K (figure 4):

$$D_{km} = \frac{d_K + D_B}{2} \tag{7}$$

Friction coefficients of the bolt thread and bearing surface of the bolt have a significant effect on the required bolt tightening torque. Sensitivity to the friction coefficient causes variation to achieved bolt pretension force, as there are differences between the surface quality of the components, and some threads may have a different amount of thread lubricant than others.

Bolt preload for 1" UNC threaded bolt that is used in this study is calculated with 700 N m tightening torque in Appendix I.

2.2 Fatigue strength of a bolt

Fatigue strength properties of a material can be estimated by using different fatigue diagrams, which show fatigue limits for different stress amplitudes and mean stress levels. Fatigue limit diagrams are usually created by testing polished test samples at room temperature. However, machine components usually have shapes that create a notch effect, surfaces have roughness, and parts are used in environments that will reduce the fatigue life of the component.

From the loading point of view, the lifetime of a component under fatigue loading is not dependant only on the stress amplitude, but it also depends on the mean stress level σ_m and whether the load type is tensile or compressive. Dynamic load type is considered as alternating stress when stress varies between tension and compression during the load cycle. When the stress does not vary from tension side to compression or vice versa, load type is called pulsating load. The load type shown in figure 8 is pulsating load.

Type of the dynamic loading can be described with stress ratio R, which is calculated by maximum and minimum stresses of the load cycle using the following formula (Budynas, Nisbett 2011, p. 302).

$$R = \frac{\sigma_{\min}}{\sigma_{\max}} \tag{8}$$

When load type is fully alternating, the value for stress ratio R is -1. Midrange stress σ_m value is zero with a fully alternating load. Stress ratio R is higher than 1 in pulsating load types where the stress state remains at the compressive side in all phases of the load cycle.

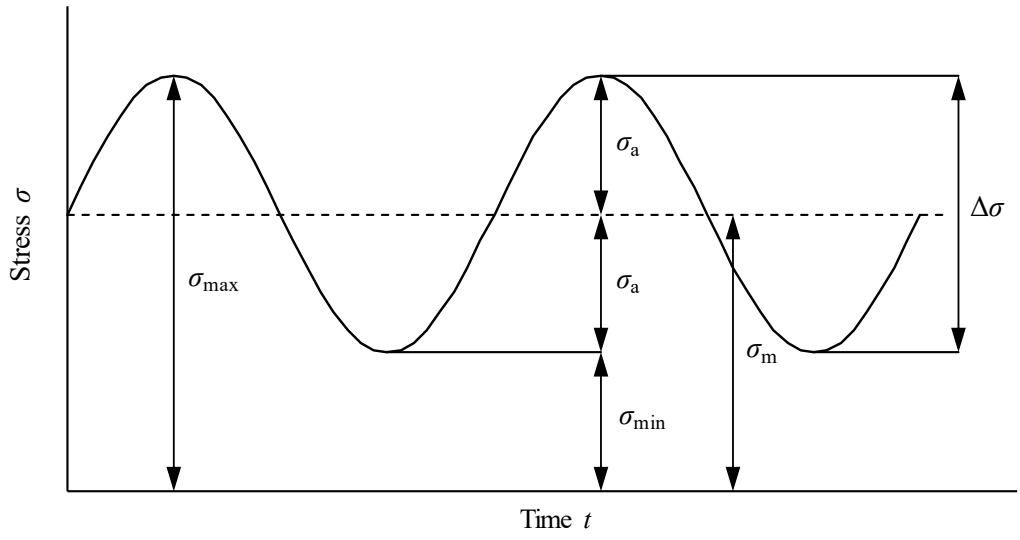

Figure 8. Stress components on a Stress-Time plot (Modified from SFS 3099, 1974, p. 2).

Table 8. Abbreviations of figure 8.

σ_{max}	Maximum stress	σ_m	Mean stress
σ_{min}	Minimum stress	σ_a	Stress amplitude
$\Delta\sigma$	Stress range		

2.2.1 Goodman-Smith diagram

Figure 9 shows the Goodman-Smith type of fatigue limit diagram where the diagonal dashed line represents mean stress σ_m. Theoretical fatigue limit for an infinite number of load cycles is within the boundary that is formed by the yield strength of the material R_e, fatigue strength limit of the material R_W, and compressive strength of the material R_{ec}. Allowed stress amplitude σ_a starts to decrease rapidly when mean stress approaches yield strength R_e of the material.

The stress amplitude limit is wider under areas of compressive mean stress. This means that the material can withstand higher stress fluctuation under compressive loading than when it is under tension load. The mean stress σ_m does not have a similar effect as a cause of progressive fracture when it is compressive stress (Smith, J. 1942).

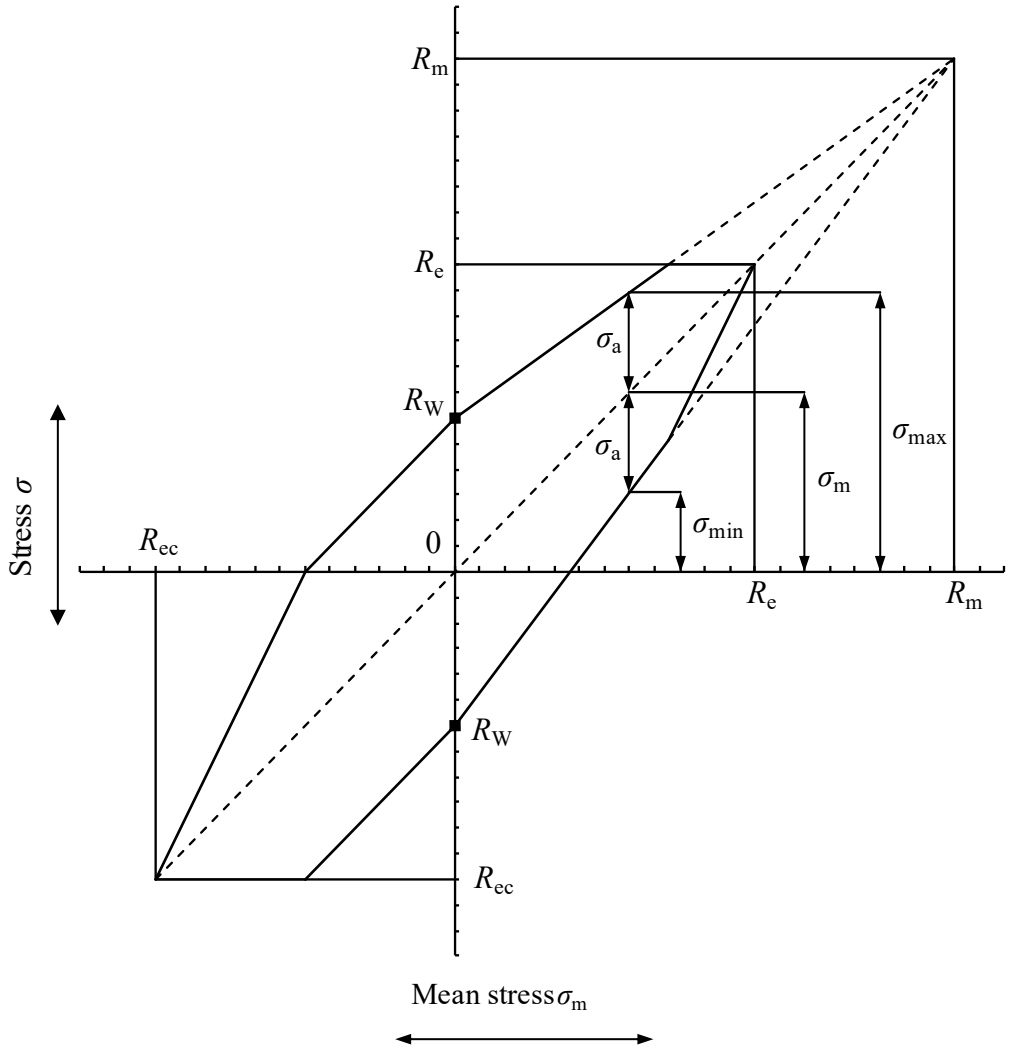

Figure 9. Goodman-Smith diagram. (Modified from SFS 3099, 1974, p. 10).

Table 9. Abbreviations of figure 9.

R_m	Ultimate tensile strength	σ_m	Mean stress
R_e	Yield strength	σ_a	Stress amplitude
R_{ec}	Compressive yield strength	$\Delta\sigma$	Stress range
R_W	Fatigue strength	σ_{max}	Maximum stress
σ	Stress	σ_{min}	Minimum stress

2.2.2 Crack growth under cyclic loading

Fracture mechanics is used to forecasting the fatigue life of the component by evaluating the crack propagation rate. Three different crack propagation modes are considered, and crack can also grow with combinations of these modes. Mode 1, shown in figure 10, is called the *opening* mode, mode 2 is the *sliding* mode, and mode 3 is the *tearing* mode. The *opening* mode 1 is the most common and severe type of these modes (Budynas, Nisbett 2011, p. 241). A test bar under tension is going to be subjected to crack propagation mode 1. Compressive stress, however, hinders the occurrence of crack opening mode 1.

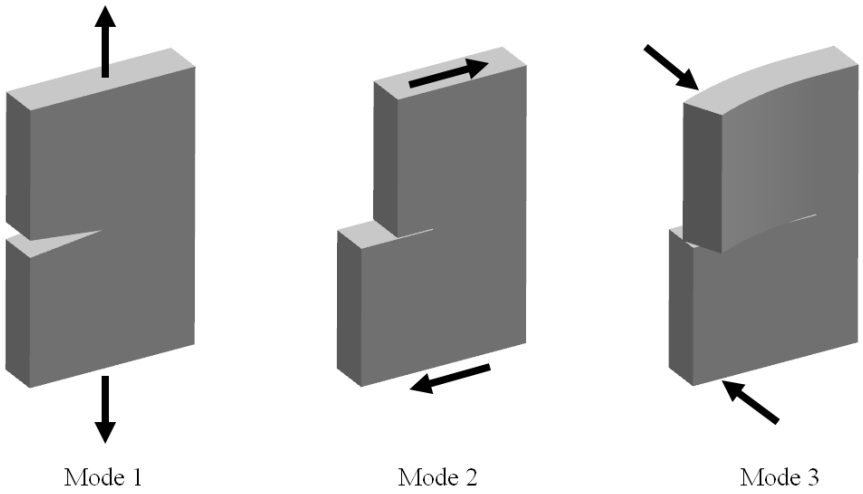

Figure 10. Crack propagation modes. (Modified from Sagheer, A. 2013, p. 48).

Eurocode 3 standard 1-9 for steel structures and fatigue loading, accounts for compressive stress of the dynamic load such that only 60% of the compressive stress is considered as effective when equivalent peak to peak stress amplitude $\Delta\sigma$ is determined (Eurocode 3: Design of steel structures - Part 1-9: Fatigue). This means that if for unidirectional tensile stress with a stress ratio of $R=0$, stress range $\Delta\sigma$ is 100 MPa, for alternating load with a stress

ratio of $R = -1$ and same 100 MPa actual stress range, the effective stress range is considered to be only 80 MPa because the second half of the peak-to-peak amplitude is under compression.

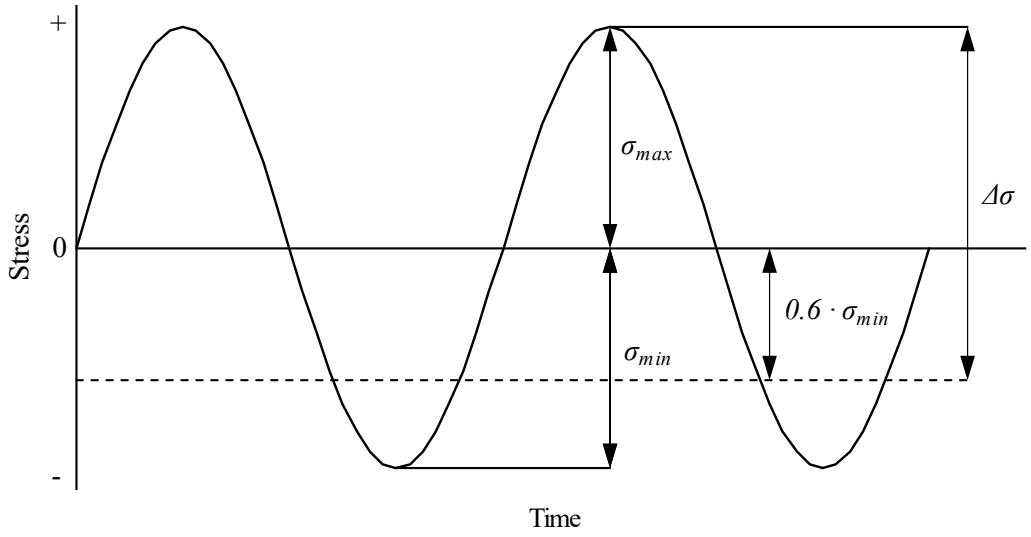

Figure 11. Modified stress range (Image modified from Eurocode 3: Design of steel structures - Part 1-9: Fatigue).

Fatigue can take place in the structure even if the external loading is compressive in all phases of the load cycle because there can be local areas where shearing occurs, or a tensile stress state is reached due part geometry or residual stresses. There are the following possibilities for fatigue failure of a bolt that is subjected to pulsating compressive loading:

- Shearing of threads.
- Shearing of the bolt head.
- Cracking failure of the bolt shank if the root of the thread reaches tensile stress state at some part of the load cycle.
- Fretting fatigue damage of thread flanks.

2.2.3 Stress concentration factor of threads

Geometric discontinuities in the shape of the component cause elevated stress levels in those localized areas under the load when compared to nominal stress σ_o of the cross-section. This

effect is described as stress concentration factor K_t which can be determined by using the following formula (Budynas, Nisbett, 2011, p. 111).

$$K_t = \frac{\sigma_{max}}{\sigma_0} \quad (9)$$

In a threaded joint, the stress concentration factor (SCF) value also depends on how many load-bearing threads does the joint have. Stress concentration will be higher with fewer threads in contact.

Threaded joint under fatigue loading usually cracks from the first two threads because they are taking 45% of the load (Hobbs 1998, p. 6). Special types of nuts have been developed for fatigue-loaded bolted joints that will flex under the load differently than standard nuts, distributing the load more evenly to several threads. Another way of smooth the load between several threads is to use slightly tapered threads. The approach of tapering the threads to reduce the stress concentration factor is studied with finite element analysis in chapter 4.4 of this research work.

The stress concentration factor of threads depends largely on the thread profile. A larger root radius of thread will lead to reduced stress concentration; hence the finer pitch threads perform typically worse under fatigue loading than coarse threads. Special thread profiles have been introduced for fatigue-loaded bolted joints. Such thread profiles for improved fatigue life are UNR- and MJ (ISO 5855-1) threads, which both specify root radius *c* of the thread shown in figure 1. The stress concentration factor of 1" UNC threads is analyzed with the finite element method in chapter 4.

Stress concentration factor K_t is also dependant on the load condition. Stress levels at the notch root are affected by additional bending moment or torsional loads.

2.2.4 Buckling of the bolt

Beam under compressive load may become unstable if the second moment of area *I* of the cross-section is not enough for the length and load that the bolt is subjected to. Critical load

for buckling can be determined by using Euler's column formula (Budynas, Nisbett 2011, p. 182).

$$P_{\text{cr}} = \frac{C\pi^2 EI}{L^2} \tag{10}$$

Table 10. Abbreviations of formula 10.

P_{cr}	Critical load
C	Condition constant taking into account the boundary conditions of the beam
E	Young's modulus
I	Second moment of area
L	Length

End condition constant C depends on what type of constraints does the compressed column has on ends. Critical load P_{cr} is sensitive to whether rotations and translations of the column ends are fixed or not. Four different end condition constants of the column are illustrated in figure 12.

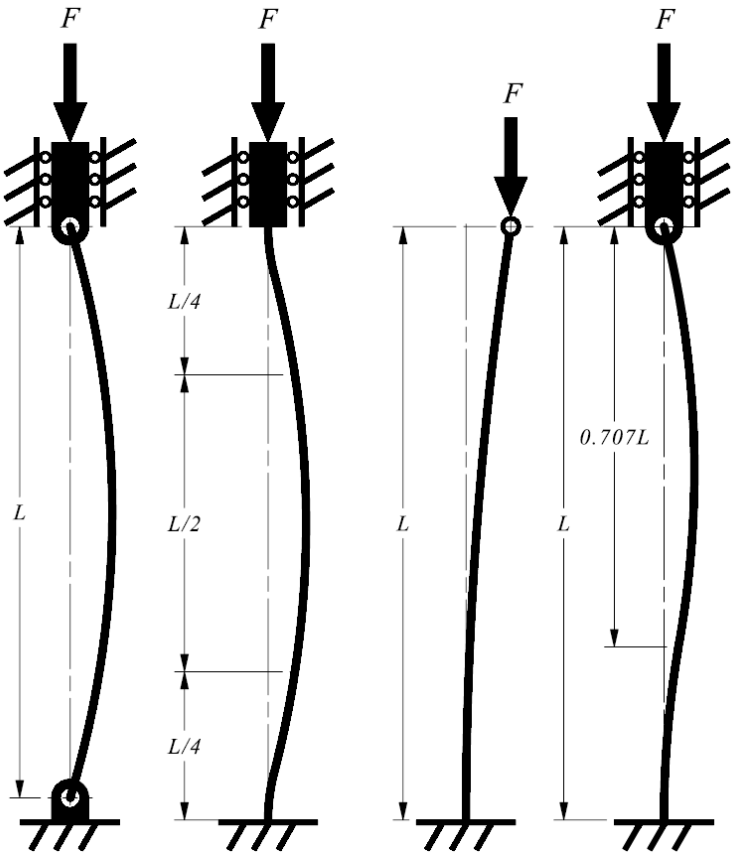

Figure 12. End condition constant values *C* of different end restraints of the column. From left to right: *C* = 1, *C* = 4, *C* = 1/4, *C* = 2. (Modified from Budynas, Nisbett 2011, p. 182.)

The theoretical end condition constant value for the bolted joint of the study is 1/4, as the load is applied to the unsupported bolt head and the nut is fixed to the ground. The diameter of the bolt that is studied in this research is a nearly equal dimension to the length of the unsupported shank of the bolt, which means that buckling of the bolt is not expected. The buckling load of the bolt is calculated in Appendix II.

2.2.5 Strain-life fatigue analysis

The lifetime of fatigue-loaded structure can be predicted by stress, strain, and fracture mechanics. With the stress-life (*S*-*N*) method, stress level *S* is used to predict the number of load cycles *N* the part will withstand before failure. The stress-life method is best suitable with high cycle fatigue applications, where $N > 10^3$ and where stress levels remain in the elastic region of the material. The stress-life method is not accurate in cases where stress levels go to the plastic region of material due to stress concentration factors of the part, for

example. Local plastic deformation of the material causes a nonlinear relationship between stress and strain. Multiplying nominal stress with stress concentration factor K_t will result in inaccurate stress values of the notch tip when the yield strength of the material is exceeded.

With the strain-life (ε-N) method, instead of stress variation, strain ε is used for estimating crack nucleation time. The strain-life method does not predict crack propagation time which is calculated by using fracture mechanics. However, in many fatigue-loaded structures, it is the crack nucleation time that determines the lifetime of the component, and crack propagation time to component failure can be relatively short after the crack has initiated to the structure.

The strain-life method is suitable for estimating component lifetime in loading scenarios where local plastic deformation of the material occurs at the notch tip. This plasticity effect is considered in the material-dependent fatigue notch factor K_f (Budynas, Nisbett 2011, p. 295).

$$K_f = 1 + q(K_t - 1) \tag{11}$$

Where q is notch sensitivity which is determined by material constant a and notch radius ρ (Airila et al. 2010, p. 38.)

$$q = \frac{1}{1 + \frac{a}{\rho}} \tag{12}$$

Material constant value a for steels can be approximated by the tensile strength of the material. Table 11 shows approximated material constant values with different strength class steels.

Table 11. Material constant value a approximation based on tensile strength R_m. (Airila. et al. 2010, p. 38.)

Tensile strength R_m [MPa]	Material constant a [mm]
400	0.33
600	0.20
800	0.14
1000	0.10
1200	0.06
1400	0.05
1600	0.04

Local stresses stop being proportional to strains after stress levels reach the yield strength of the material. The yielding of the material can be inspected by comparing stress concentration factor K_σ and strain concentration factor K_ε (Stephens et al. 2001, p. 211).

$$K_\sigma = \frac{\sigma}{\sigma_0} \tag{13}$$

$$K_\varepsilon = \frac{\varepsilon_l}{e} \tag{14}$$

Where ε_l is local strain at notch, e is nominal strain and σ is local stress at notch.

Stress- and strain concentration factor curves in figure 13 illustrate how the stress concentration factor starts to reduce after the material begins to yield while the strain concentration factor increases (Airila et al. 2010, p. 67).

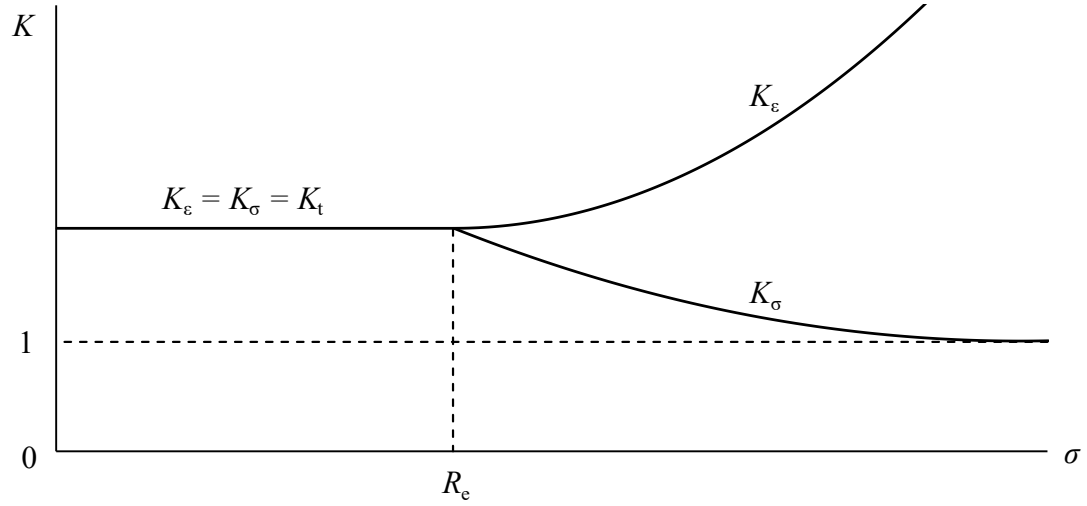

Figure 13. Stress and strain concentration factors at the yield point R_e of material. (Modified from Airila et al. 2010, p. 67).

The strain-life fatigue curve illustrated in figure 14 on a logarithmic scale consists of fatigue ductility curve ε_f', fatigue strength curve σ_f'/E, and total strain-life curve. The plastic strain portion becomes larger as the total strain grows. Failure criteria can vary from nucleation of a small crack to a certain percentage drop of tensile load.

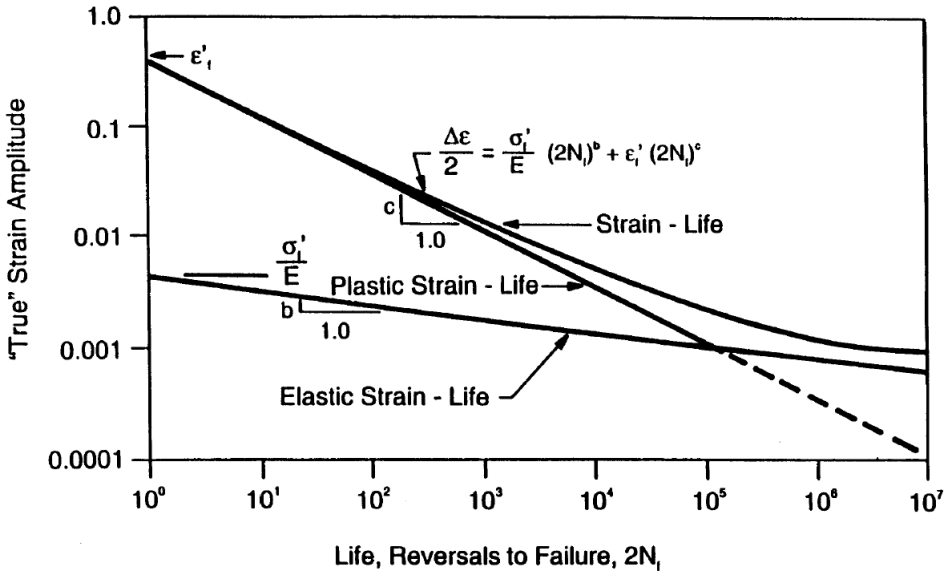

Figure 14. Strain amplitude versus reversals to failure (SAE J1099, 2002, p. 26).

2.2.6 Fretting fatigue mechanism

The fretting fatigue phenomenon occurs when two contacting surfaces slip against each other repeatedly with a small amplitude, creating fatigue cracks to the material. Major contributors to the fretting fatigue strength are clamping pressure, the amplitude of slipping, and the friction coefficient of the contact pair (Attia, Waterhouse 1992, p. 16). Fretting fatigue occurs typically on thread flanks, and it is usually caused by insufficient make-up torque (Brennan 1992, p. 107). This means that reduced bolt preload can lead to fretting fatigue problems.

The maximum force that friction pair can transfer without slipping is determined by the normal force F_n and friction coefficient μ (Hills 1994, p. 42). High frictional force Q values accelerate crack initiation by fretting. Slipping of the contact pair may increase the friction coefficient significantly, thus leading to elevated shear forces and crack initiation:

$$Q = F_n \mu \tag{15}$$

Fretting damage may occur with as small displacement amplitudes as 1 µm. Fretting fatigue life is lowest at the mixed stick-slip regime, which is at the boundary region of gross slip and mixed stick and slip conditions (Vingsbo, Söderberg 1988, p. 142). The mixed stick-slip condition is also known as the partial slip condition.

The relationship of displacement amplitude and fatigue life shown in figure 15 demonstrates how the fatigue life rapidly drops in the transition area between partial slip and gross slip displacement. The wear of surfaces increases with the displacement amplitude, and the wear slope grows when moving from partial slip to the gross sliding regime.

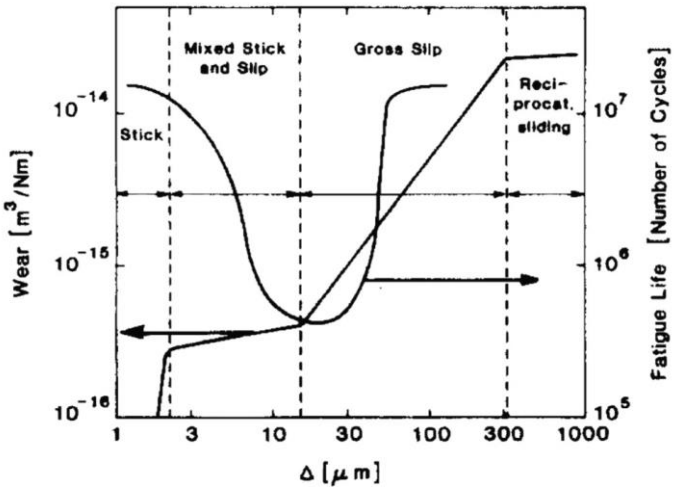

Figure 15. Fretting map (Vingsbo, Söderberg 1988, p. 142).

3 FINITE ELEMENT ANALYSIS OF THE BOLT JOINT

Finite element analysis enables to study and to compare the effect of varying load scenarios and geometrical differences of threaded connection to stress- and strain concentration factors. The stress concentration factor of threads can be determined by comparing nominal stress values of the bolt shank to the peak stress values of the thread root. Strain concentration factor is studied with using elastic-plastic material model in cases where yield strength of the material is exceeded.

3.1 Methodology used with finite element analysis

- A three-dimensional model of the threaded connection is created with an accurately detailed 1” UNC thread profile of the bolt and the nut. Section of this model is used for the two-dimensional stress analysis. Local stress values of the two-dimensional simulation model are expected to be on a conservative side when compared to the actual three-dimensional part.
- The effect of eccentric loading on stress concentration factors of the bolt is examined.
- The effect of the friction coefficient between thread flanks on stress concentration factors of the bolt is examined.
- Three different thread engagement lengths are compared with the standard thread profile.
- Tapered threads of the bolt are studied and compared to standard non-tapered thread profile.
- The bolted joint is studied with three different bolt loads. Two of the bolt load values represent different bolt preloads, and one value represents bolt load when an external load is applied to the bolt joint. The critical location of the threads is located by examining maximum principal stresses of the joint, and strain values are captured from that location for strain-life fatigue analysis.

3.2 Simulation model of the bolted joint

Stress concentration factors of the bolt are studied with Ansys 2020 R2 software. The simulation model consists of 8-node quadratic elements. This element type has four corner nodes and four mid-side nodes. The benefit of this type of element is that it provides

improved accuracy for curved boundaries, which in this case can be found from the thread roots of the simulation model. Surface-to-surface type of contact is being used between threads of the bolt and nut with different friction coefficient values to inspect what sort of impact sliding has to stress levels at the root of the thread. Simulations are run with 20 substeps. Figure 16 shows the two-dimensional simulation model.

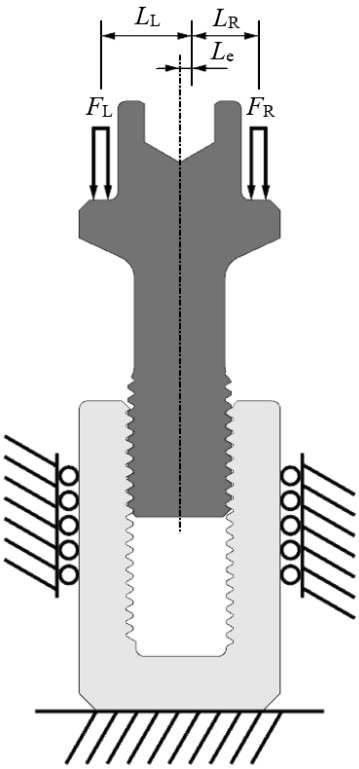

Figure 16. Supports and external loads of the two-dimensional FEA-simulation model.

The cross-section in figure 16 illustrates how sidewalls of the nut are supported with frictionless supports and how the nut face has been fixed to the ground. Threads of the bolt and the nut are connected by frictional contacts. An external force is applied to the joint by two separate bearing faces F_L and F_R. In the symmetric load case $F_L = F_R$, and in eccentric load cases $F_L < F_R$.

The thickness parameter t_1 is adjusted so that the corresponding target load of the actual three-dimensional bolt is achieved.

The centerline of applied loads is the point where counterclockwise and clockwise moments are in equilibrium:

$$F_{\mathrm{L}}L_{\mathrm{L}} = F_{\mathrm{R}}L_{\mathrm{R}} \tag{16}$$

Load eccentricity distance L_{e} is calculated by the following formula:

$$L_{\mathrm{e}} = \frac{L_1F_{\mathrm{R}} - L_1F_{\mathrm{L}}}{2F_{\mathrm{R}} + 2F_{\mathrm{L}}} \tag{17}$$

Where L_1 is the distance between center points of load bearing faces:

$$L_1 = L_{\mathrm{L}} + L_{\mathrm{R}} \tag{18}$$

3.2.1 Bending stress component in eccentric loading

When yield strength of material is not exceeded, strain ε can be calculated by stress σ and Youngs modulus E of the material (Outinen, Salmi, 2004, p. 38.)

$$\varepsilon = \frac{\sigma}{E} \tag{19}$$

Stress σ at the shank of bolt consists of normal stress component σ_0 and bending stress component σ_{b} (Outinen, Salmi, 2004, p. 193. abbreviations changed)

$$\sigma = \sigma_0 + \sigma_{\mathrm{b}} = \frac{F}{A} + \frac{M}{W} \tag{20}$$

Where A is the cross-sectional area of the bolt, M is the internal bending moment and W is the section modulus of bolt shank. Stress components are shown in figure 17 below.

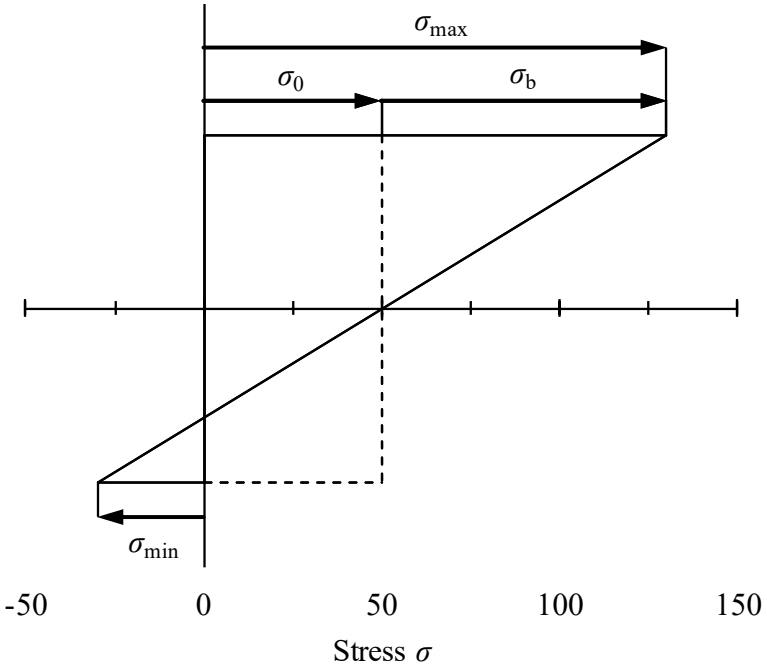

Figure 17. Maximum stress σ_{max}, minimum stress σ_{min}, normal stress component σ_0 and bending stress component σ_b. Symmetric cross-section of the bolt. (Modified from Outinen, Salmi 2004, p. 193.)

Neutral axis shifts offset from centerline of the bolt when both bending stress component σ_b and normal stress component σ_0 are present in the structure.

Normal stress is equal to the average value of maximum stress and minimum stress when the cross-section is symmetric, and measurement points are on opposing sides of the beam.

$$\sigma_0 = \frac{\sigma_{max} + \sigma_{min}}{2} \tag{21}$$

Bending stress component σ_b can be calculated by subtracting normal stress from total stress:

$$\sigma_b = \sigma - \sigma_0 \tag{22}$$

When maximum stress σ_{max} and minimum stress σ_{min} are below yield strength limit R_e of material, bolt load F_S can be calculated by multiplying normal stress σ_0 with the cross-sectional area of bolt shank A_3:

$$F_S = \sigma_0 \cdot A_3 \tag{23}$$

3.2.2 Coding scheme of simulation models

Two-dimensional FEA simulations are run with three different load eccentricity values and three different friction coefficient values to compare various load conditions. A coding scheme is used with different simulation runs. The coding scheme shown in figure 18 consists of material model type prefix, corresponding external load of a three-dimensional bolt, taper intersection point with bolt end, taper angle, friction coefficient, number of engaged threads, and load eccentricity distance. Prefix LE stands for “linear-elastic,” and prefix EP stands for “elastic-plastic”.

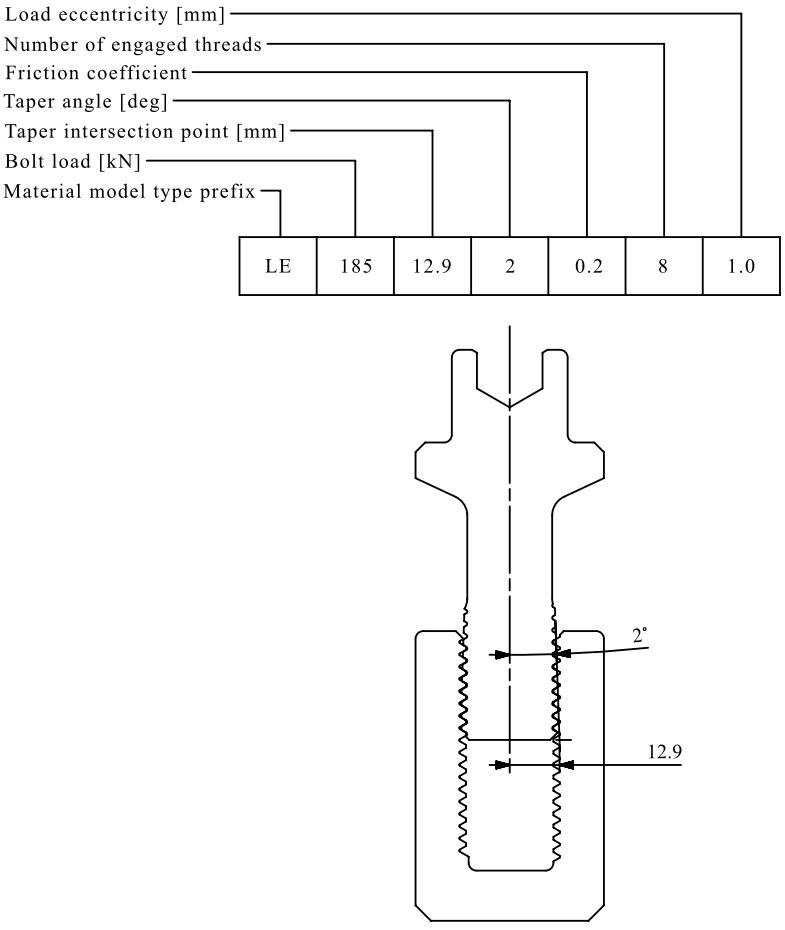

Figure 18. Coding scheme of FEA-simulation models.

Table 12. Simulation parameters of two-dimensional FE-analysis of a non-tapered bolt with the linear-elastic material model. Thickness parameter t_1 = 0.917 mm.

Simulation model	Force F_L [N]	Force F_R [N]	Friction coefficient μ	Load eccentricity L_e [mm]
LE-185-12.7-0-0.10-8-0.0	5000	5000	0.10	0.0
LE-185-12.7-0-0.10-8-1.0	4742	5258	0.10	1.0
LE-185-12.7-0-0.10-8-2.0	4485	5515	0.10	2.0
LE-185-12.7-0-0.15-8-0.0	5000	5000	0.15	0.0
LE-185-12.7-0-0.15-8-1.0	4742	5258	0.15	1.0
LE-185-12.7-0-0.15-8-2.0	4485	5515	0.15	2.0
LE-185-12.7-0-0.20-8-0.0	5000	5000	0.20	0.0
LE-185-12.7-0-0.20-8-1.0	4742	5258	0.20	1.0
LE-185-12.7-0-0.20-8-2.0	4485	5515	0.20	2.0

Thread identification b_{L1} shown in figure 19 means root of the first thread of the left-hand side of the bolt. Abbreviation n_{R1} stands for the first root of the nut on the right-hand side, and f_{L1} means flank contact of the thread. Stress concentration value K at the root of the first contacting thread of the bolt on the right-hand side is coded as K_{bR1} and so on. Even with the symmetric load case, stress concentration values are slightly different on the left-hand side and right-hand side because the cross-section is created from a 3d-model. This is because thread flanks are on different heights by half of the pitch on either side of the bolt, as with a real part.

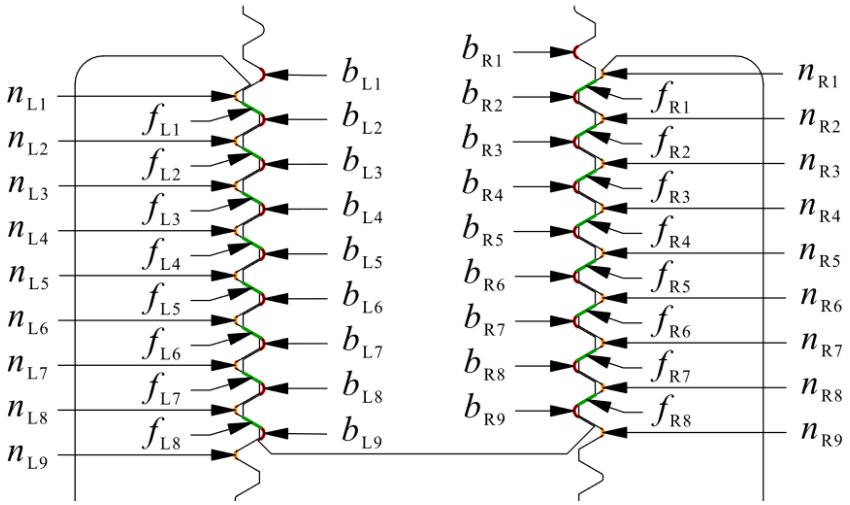

Figure 19. Abbreviations of roots and contacting flanks of threads.

3.2.3 Nominal stress determination of the bolt

Nominal stress value σ_0 is determined by external forces F_L, F_R, minor diameter d_1 of the bolt, and thickness parameter t_1 (Appendix III). When nominal stress σ_0 and maximum stress σ_{max} are known, stress concentration factor K_t can be calculated (formula 9).

Nominal stress σ_o of the bolt shank:

$$\sigma_0 = \frac{F_L + F_R}{d_1 t_1} \tag{24}$$

The external force of 5 kN for F_L and F_R shown in table 12 results in nominal stress σ_0 of 506 MPa, which is 56% of the yield strength of bolt material (Appendix III).

The focus of studying stress concentration factors is limited to only the eight most critical threads of the joint that have comparable contact conditions. The last thread root of the bolt does not have similar load conditions as the eight preceding threads because the last thread does not contact with nut due to the end chamfer of the bolt. Simulation runs with reduced number of engaged threads are created by suppressing thread contacts. For simulation model LE-185-12.7-0-0.10-6-0.0 contacts f_{L8}, f_{R8}, f_{L7} and f_{R7} of last two contacting threads are suppressed.

3.2.4 Linear elastic material model

Material of bolt and nut is quenched and tempered steel with 10.9 strength class. Linear elastic material properties used in FEA simulations are shown in table 13 below.

Table 13. Linear elastic material properties of bolt used in FEA-simulations.

Part	Poisson's ratio ν	Young's modulus E [GPa]	Yield Strength R_e [MPa]	Tensile Strength R_m [MPa]
Bolt	0.3	200	900	1000
Nut	0.3	200	900	1000

3.3 Mesh accuracy

The simulation model consists of 8-node quadratic elements. This element type has four corner nodes and four mid-side nodes. The benefit of this type of element is that it provides improved accuracy for curved boundaries, which in this case can be found from the thread roots of the simulation model.

The mesh size of main bodies of the bolt and the nut is 1.0 mm and 0.02 mm on the surface of threads. Mesh of the simulation model is shown in figure 20.

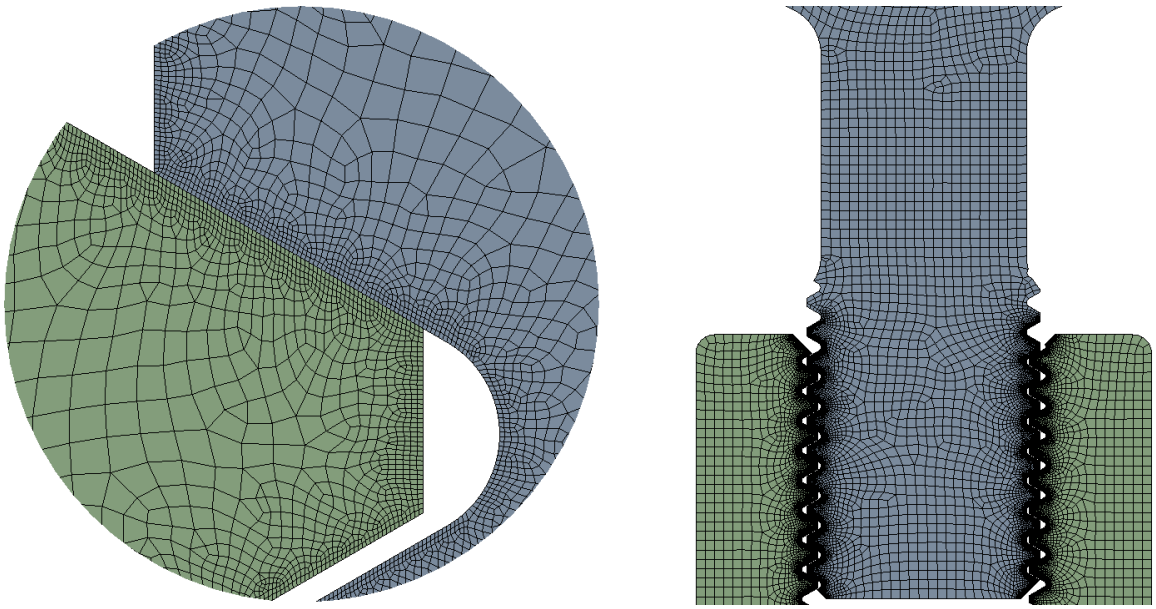

Figure 20. Mesh at surface of threads consists of 0.02 mm 8-node quadratic elements.

The sufficiency of accuracy of the mesh can be examined by looking into peak nodal stress values at the root of the thread and by inspecting how much there is a variation with stress values of nodes at peak stress areas. Linear elastic material model is used so that the yielding of the material doesn't limit the maximum stress values. Variation of nodal stress values at peak stress area in the root of the thread shown in figure 21 is below one percent, which suggests that there aren't singularities in this area of the simulation model.

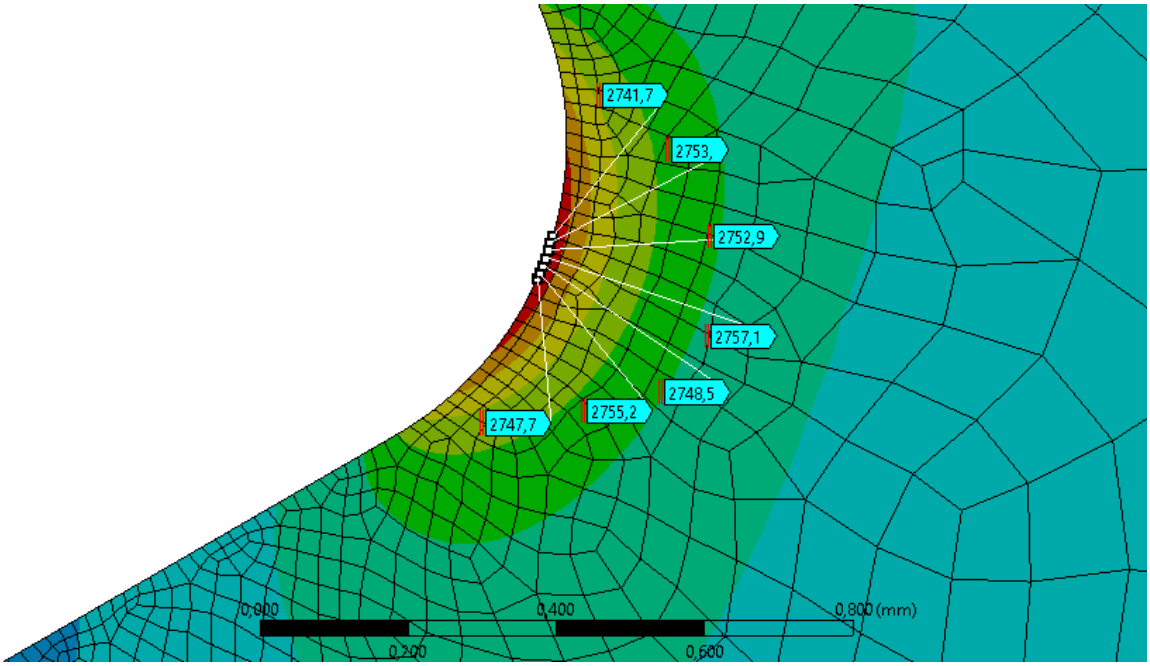

Figure 21. Stress variation between nodes at root of the thread.

3.4 Maximum principal stress study of threads

Maximum principal stress values of bolt and nut are examined to find locations where compression-loaded bolt reaches tensile stress state. As an example, figure 22 illustrates maximum principal stress levels at the root of several threads of the bolt. Location b_{R9} shows high maximum principal stress levels, which means that this is an area of interest if strain-life fatigue analysis is to be applied to evaluate the fatigue life of the joint.

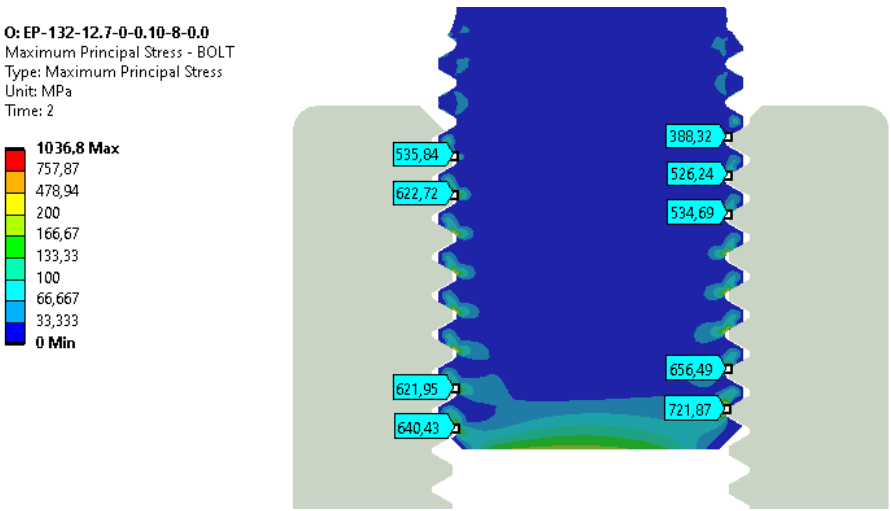

Figure 22. Maximum principal stress at threads of the bolt.

3.5 Shear stress study of threads

Maximum shear stress values of bolt threads are inspected from two possible shear paths through the thread shown in figure 23. Another shear path is at the root where contact ends with the thread of the nut. The second shear path is through the middle of a flank of the bolt thread. Averaged nodal stress values $\tau_{max,flank}$, and $\tau_{max,root}$ through shear paths are captured.

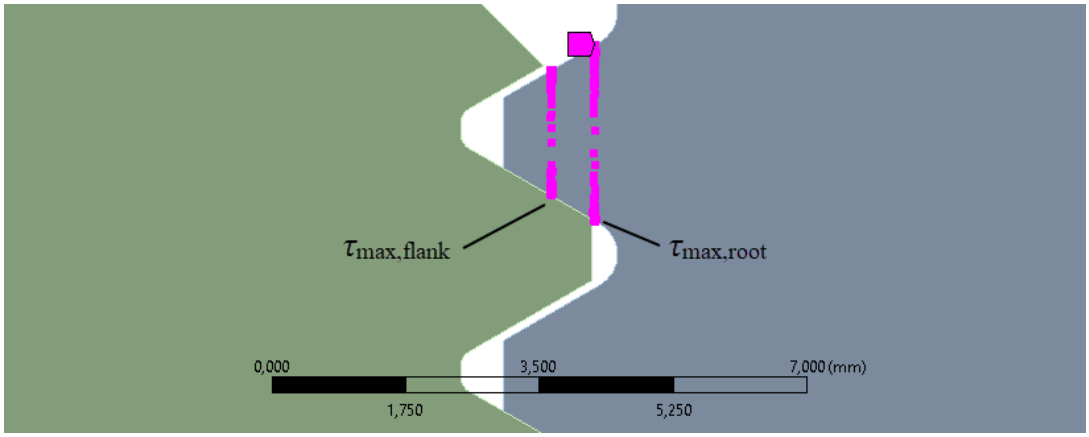

Figure 23. Two different shear paths through the bolt thread.

3.6 Bilinear elastic-plastic material model

The majority of simulations are run with an elastic-plastic material model. The linear elastic material model is used for studying the impact of friction coefficient and the general effect of eccentric loading on the stress concentration factor of bolt threads. Comparison of different thread geometries and thread engagement lengths is performed by a more accurate elastic-plastic material model so that the yielding effect of the material is considered with simulations.

Strain concentration factor K_ε is inspected by using a simplified bilinear elastic-plastic material model, which includes elastic and plastic regions. With a perfectly plastic material model, the stress-strain curve is horizontal in the plastic region. However, with steel materials, usually, some strain hardening occurs after the yield strength limit of the material has been reached. The strain hardening effect is considered in the bilinear material model by determining tangent modulus E_t for the plastic region. Available material data is used for estimating tangent modulus in the plastic region [Matdat d.o.o. 2021]. The same tangent modulus shown in figure 24 is used with material curves of both parts.

Table 14. Parameters of bilinear material model used with finite element analysis.

Part	Poisson's ratio v	Young's modulus E [GPa]	Yield Strength R_e [MPa]	Tangent Modulus E_t [MPa]
Bolt	0.3	200	900	8000
Nut	0.3	200	900	8000

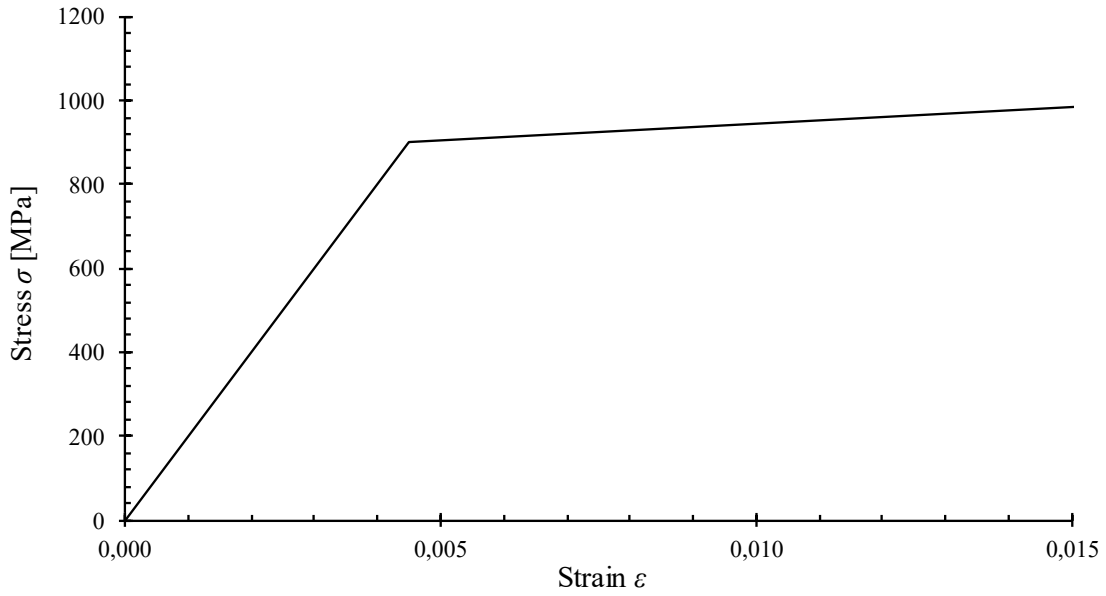

Figure 24. Bilinear elastic-plastic material curve of bolt used with finite element analysis.

4 STRESS AND STRAIN CONCENTRATION FACTOR COMPARISON OF THREADS

This stress study is mainly focused on the bolt side of the threaded joint. The pitch diameter of a 1” UNC nut is approximately 1% larger than the pitch diameter on the bolt side, which does not create a large inaccuracy to two-dimensional simulation results when stress levels of either side of the joint are inspected.

4.1 Eccentric loading of the bolt

Eccentric load adds a bending moment to the bolt, increasing compressive stress on the right-hand side while reducing compressive stress on the left-hand side of the bolt. This effect can be observed in figure 25, which shows how the stress distribution of the joint is affected by the load eccentricity.

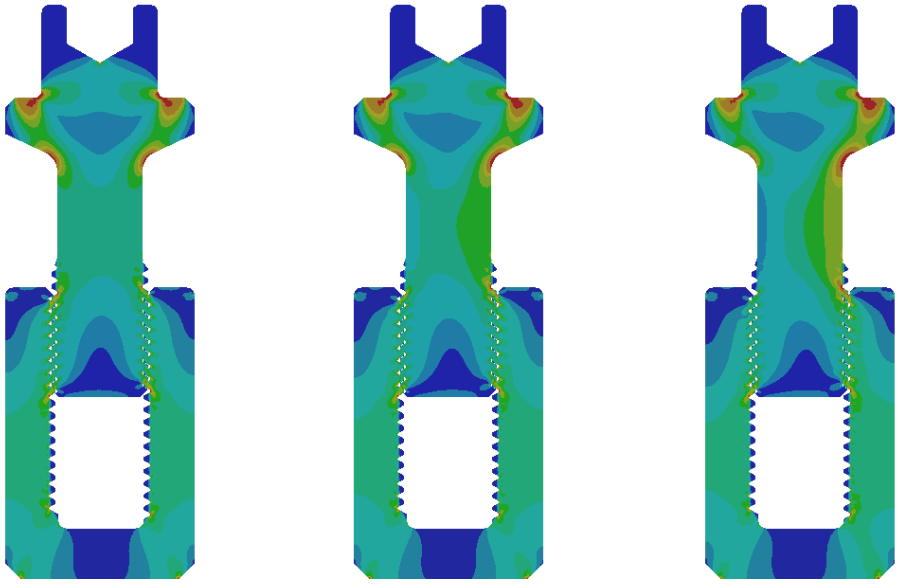

Figure 25. Effect of the eccentric load condition to the Von Mises stress distribution of the bolt joint. μ = 0.1, F_S = 185 kN. From left to right: L_e = 0.0, L_e = 1.0, L_e = 2.0.

K_t values shown in figure 26 are stress concentration factors K_{bL1}…K_{bL9} on the left side of the bolt and values on the right side of the graph are stress concentration factors K_{bR1}…K_{bR8} on the opposite side of the bolt. The graph shows how the stress concentration factor on the

thread root increases on the right-hand side of the bolt while reducing on the left-hand side when external load eccentricity distance L_e grows.

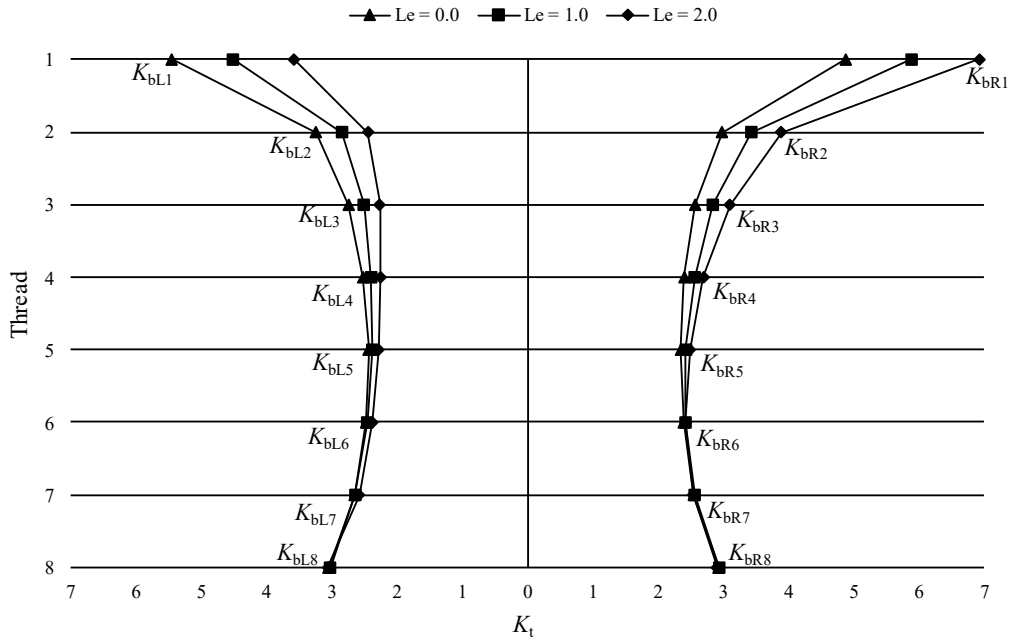

Figure 26. Stress concentration factor of thread roots with different load eccentricity values. Linear elastic material model. $\mu = 0.1$, $F_S = 185$ kN.

4.2 The friction coefficient between thread flanks

Effect of friction coefficient is studied with symmetric load, two different friction coefficient values, and with a linear elastic material model. The friction coefficient does not appear to have a meaningful effect on stress concentration values of thread roots with identical bolt loads. However, friction coefficient has a significant effect to the achieved bolt preload if same bolt tightening torque is applied.

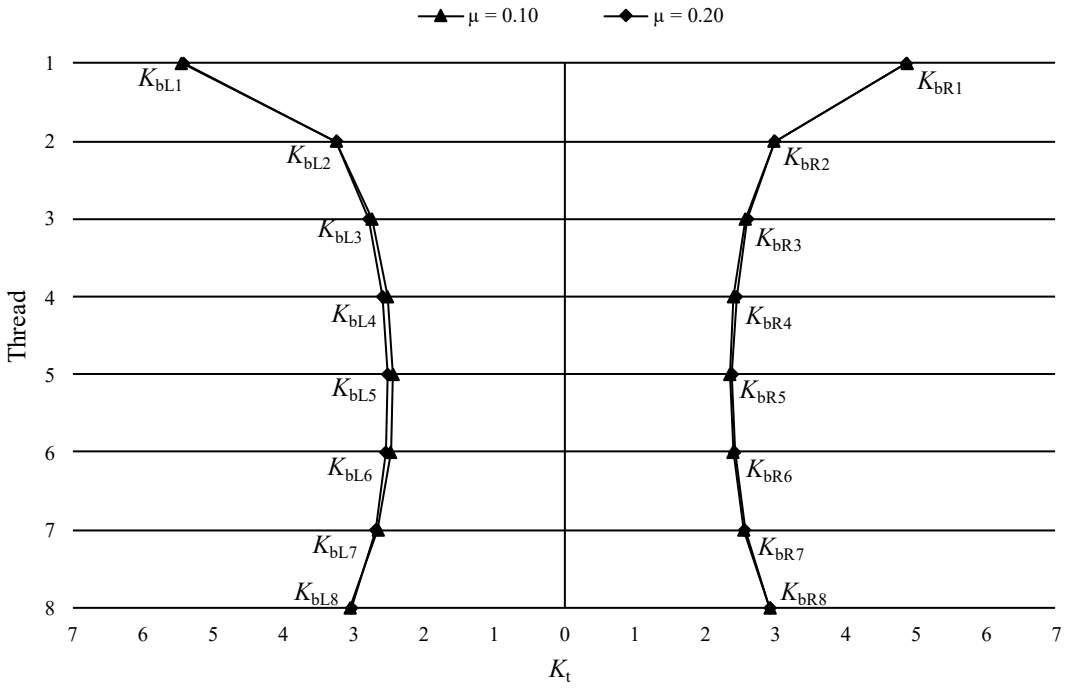

Figure 27. Stress concentration factor of bolt thread roots with two different friction coefficient values. Linear elastic material model. F_S = 185 kN.

4.3 Thread engagement length

Three different thread engagement lengths of 8, 7, and 6 engaged threads are studied with both linear elastic and bilinear elastic-plastic material models using symmetric 185 kN bolt load. Stress- and strain concentration factors are determined, and maximum shear stress values from the root and flank of threads are inspected.

The number of engaged threads has a noticeable effect on stress concentration values at the root of the threads as seen in figure 28. The difference between six to seven engaged threads is slightly larger than the difference between seven and eight engaged threads.

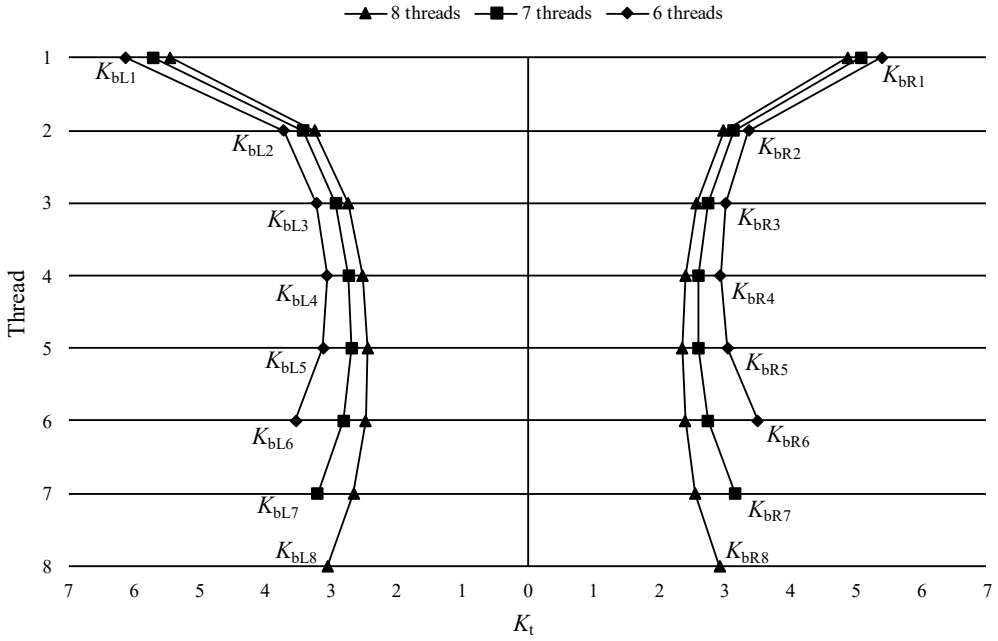

Figure 28. Stress concentration factor of bolt thread roots with different number of engaged threads. Linear elastic material model. $F_L = F_R = 5$ kN, $t_1 = 0.917$ mm, $\mu = 0.1$, $F_S = 185$ kN.

Table 15 contains total strain values ε at the root of the bolt thread and averaged maximum shear stress values $\tau_{max,root}$ and $\tau_{max,flank}$. Total strain at root of the thread is inspected instead of Von Mises stress values because the yield strength limit of the material is exceeded with an elastic-plastic material model.

Table 15. Strain values of root and maximum shear stress of the thread with different thread engagement lengths. Left-hand flank of the bolt.

		L1	*L2*	*L3*	*L4*	*L5*	*L6*	*L7*	*L8*
EP-185-12.7-0-0.10-8-0.0	ε_{root}	2.81E-2	1.19E-2	9.07E-3	7.86E-3	7.40E-3	7.56E-3	8.43E-3	1.00E-2
	$\tau_{max,root}$ [MPa]	406	375	336	337	329	335	353	402
	$\tau_{max,flank}$ [MPa]	270	243	211	208	203	202	218	246
EP-185-12.7-0-0.10-7-0.0	ε_{root}	3.05E-2	1.34E-2	1.03E-2	9.21E-3	8.92E-3	9.54E-3	1.10E-3	
	$\tau_{max,root}$ [MPa]	426	401	369	375	376	402	444	
	$\tau_{max,flank}$ [MPa]	289	266	234	236	237	249	297	
EP-185-12.7-0-0.10-6-0.0	ε_{root}	3.45E-2	1.64E-2	1.28E-2	1.18E-2	1.19E-2	1.30E-2		
	$\tau_{max,root}$ [MPa]	459	438	418	432	442	485		
	$\tau_{max,flank}$ [MPa]	283	268	266	277	291	333		

The reaction force distribution of threads shown in figure 29 illustrates that the first and last threads transfer the most force to the nut. This can be explained by a compression-loaded bolted joint structure that differs from usual tension-loaded bolted joints. The fixed face of the nut is closest to the last engaged thread, which explains why the last thread also transfers a large portion of the load.

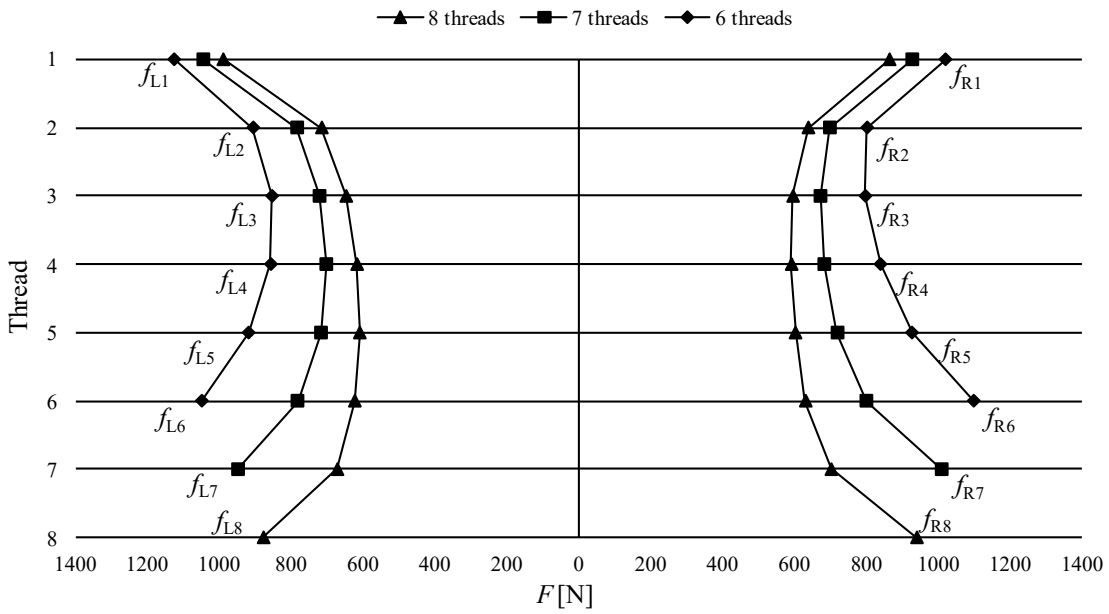

Figure 29. Reaction force distribution with different thread engagement lengths. Elastic-plastic material model. $F_L = F_R = 5$ kN, $t_1 = 0.917$ mm, $\mu = 0.1$, $F_S = 185$ kN.

Figure 30 shows averaged maximum shear stress values τ_{max} through the shear path at the root of the bolt. The two different shear paths are described in figure 23. Shear stress distribution of bolt threads differs from stress concentration factor distribution in a way that the last engaged thread has the highest shear stress levels. Simulation results are shown in table 16.

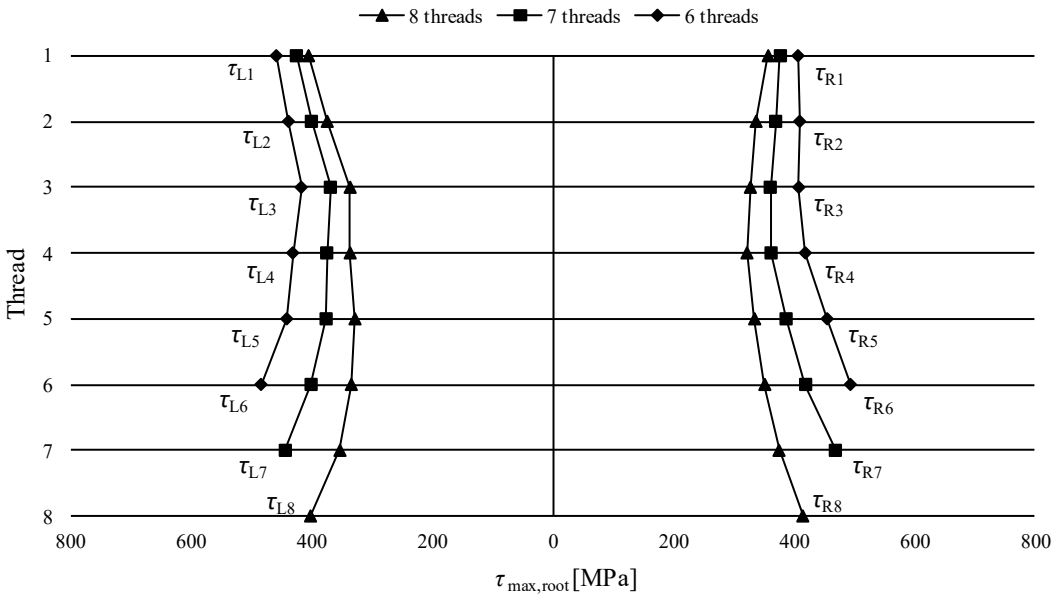

Figure 30. Maximum shear stress through root of bolt thread with different thread engagement lengths. Elastic-plastic material model. $F_L = F_R = 5$ kN, $t_1 = 0.917$ mm, $\mu = 0.1$, $F_S = 185$ kN.

4.4 Partially tapered threads

Load distribution between threads can be adjusted by modifying the thread by adding a slight taper to the otherwise standard thread. Reduced contact surface has an effect on the reaction force of the thread, but perhaps more importantly, the middle point of the contact area changes as well. When taper is added to the bolt, thread contact moves closer to the root of the thread, effectively reducing the bending moment of the bolt thread. Correspondingly, the bending moment of the nut thread increases as the middle contact point moves further away from the root of the thread.

4.4.1 Stress distribution of the bolt with tapered threads

The bolt type shown in figure 31 has been optimized for cyclic loading by adding a taper to the thread and by removing unnecessary threads from the shaft section. Reaction forces and strain concentration factors of tapered threads are studied with two different thread taper types.

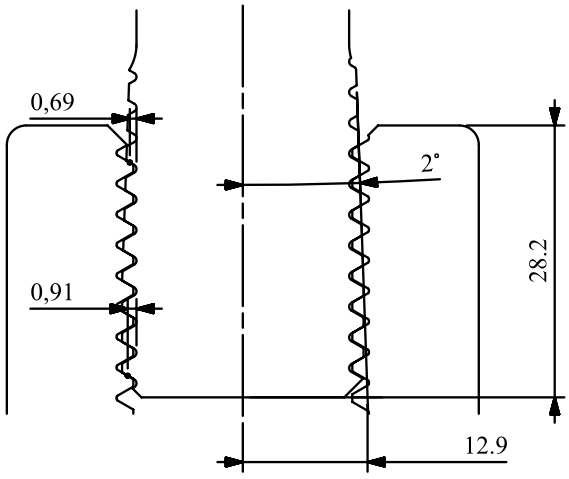

Figure 31. Middle points of two thread flanks in a bolt with tapered threads on the shaft side.

The bolt version shown in figure 31 has a taper of 2 degrees angle located such that the first four threads will have a slight taper and the last four threads remain unaffected. The second tapered model shown in figure 32 has 2 degrees taper on the last four threads of the bolt.

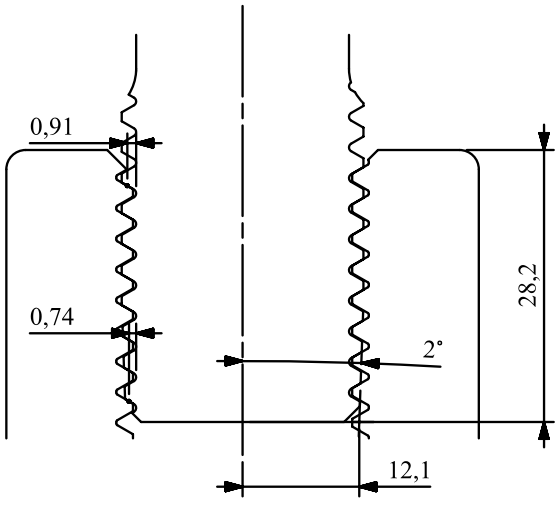

Figure 32. Middle points of two thread flanks in a bolt with tapered threads on the end of shaft.

Table 16. Strain values of root and maximum shear stress of the thread with tapered bolt threads. Left-hand flank of the bolt.

		L1	*L2*	*L3*	*L4*	*L5*	*L6*	*L7*	*L8*
EP-185-12.7-0-0.10-8-0.0	ε_{root}	2.81E-2	1.19E-2	9.07E-3	7.86E-3	7.40E-3	7.56E-3	8.43E-3	1.00E-2
	$\tau_{max,root}$ [MPa]	406	375	336	337	329	335	353	402
	$\tau_{max,flank}$ [MPa]	270	243	211	208	203	202	218	246
EP-185-12.9-2-0.10-8-0.0	ε_{root}	2.11E-2	1.10E-2	8.75E-3	8.02E-3	7.99E-3	8.04E-3	8.75E-3	1.05E-2
	$\tau_{max,root}$ [MPa]	319	321	312	313	328	327	345	388
	$\tau_{max,flank}$ [MPa]	293	238	212	213	208	219	227	253
EP-185-12.1-2-0.10-8-0.0	ε_{root}	2.83E-2	1.12E-2	9.27E-3	8.04E-3	7.58E-3	7.08E-3	7.00E-3	6.62E-3
	$\tau_{max,root}$ [MPa]	376	356	333	322	324	312	325	346
	$\tau_{max,flank}$ [MPa]	277	251	223	215	206	205	219	263

Simulation run EP-185-12.9-2-0.1-8-0.0 uses thread geometry shown in figure 31, and simulation run EP-185-12.1-2-0.1-8-0.0 uses thread geometry shown in figure 32.

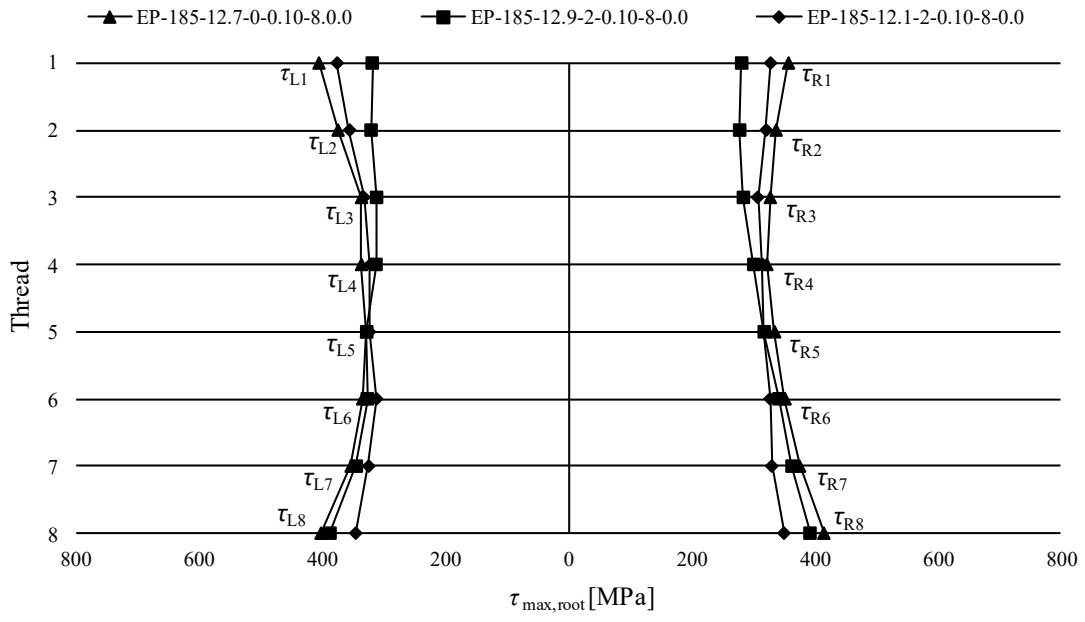

Figure 33. Maximum shear stress through root of bolt threads with two different tapered thread types. Elastic-plastic material model. $F_L = F_R = 5$ kN, $t_1 = 0.917$ mm, $\mu = 0.1$, $F_S = 185$ kN.

Figures 34 and 35 show how stress concentration at the root of the bolt thread is reduced by the taper. The most significant change occurs in the first and last threads depending on the location of the tapering.

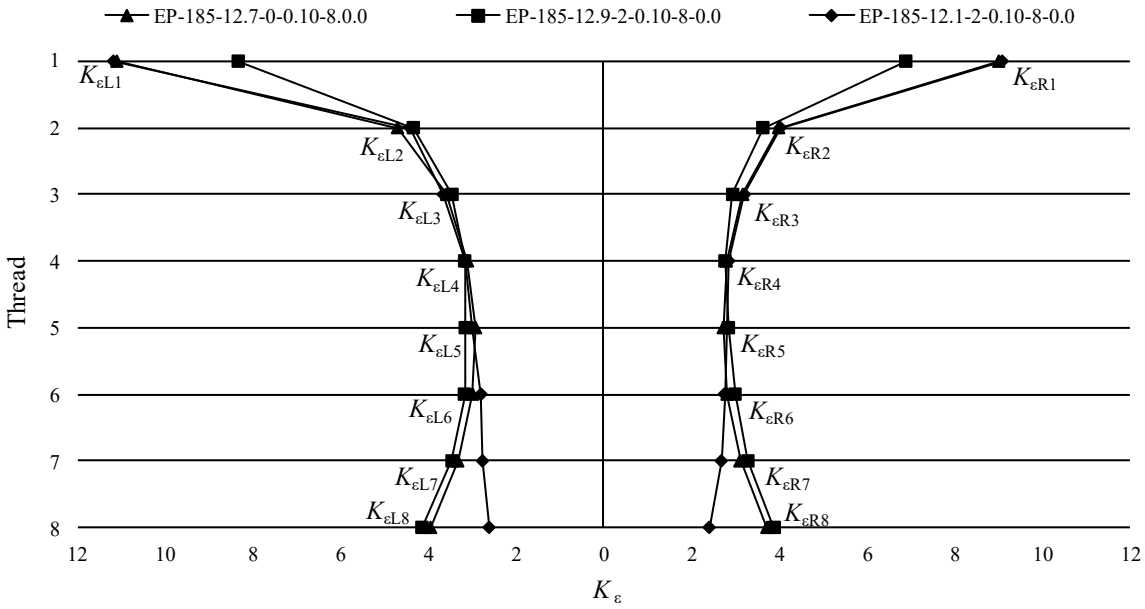

Figure 34. Strain concentration factor distribution of the bolt with two different tapered threads. $F_L = F_R = 5$ kN, $t_1 = 0.917$ mm, $\mu = 0.1$, $F_S = 185$ kN.

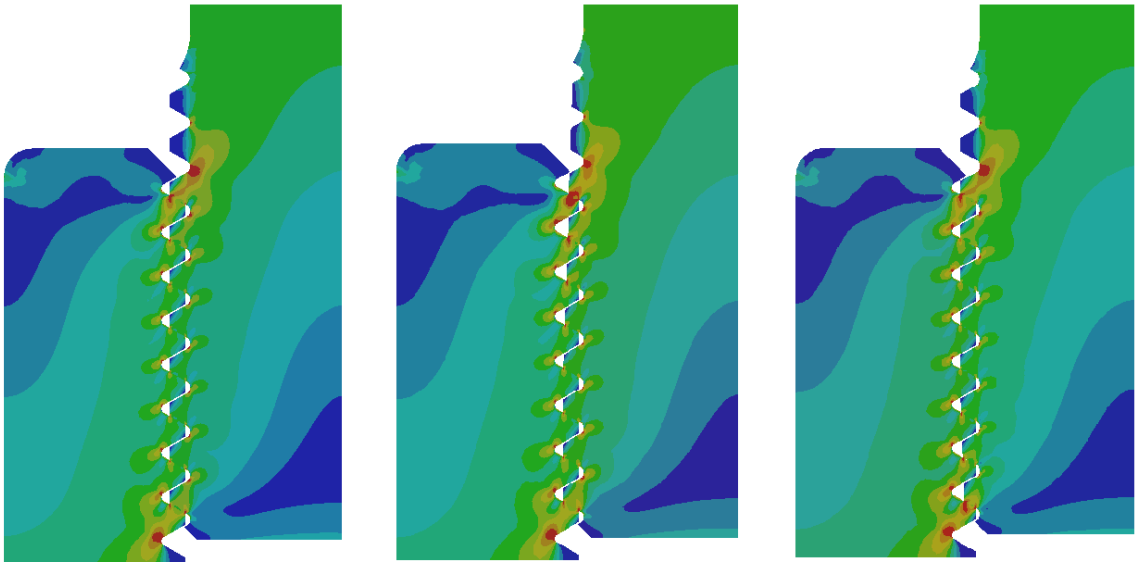

Figure 35. Effect of tapered thread to the Von Mises stress distribution of the bolt joint. From left to right: EP-185-12.7-0-0.10-8-0.0, EP-185-12.9-2-0.10-8-0.0, EP-185-12.1-2-0.10-8-0.0.

4.4.2 Stress distribution of the nut with tapered bolt

Tapered threads on the bolt have an effect on the stress levels of threads of the nut. Maximum shear stress and total strain levels of threads of nut are examined. Simulation results are shown in table 17 and figure 36.

Table 17. Strain values of root and maximum shear stress of the threads. Left hand flank of the nut.

		L1	*L2*	*L3*	*L4*	*L5*	*L6*	*L7*	*L8*
EP-185-12.7-0-0.10-8-0.0	ε_{root}	8.07E-3	1.98E-2	1.58E-2	1.42E-2	1.26E-2	1.42E-2	1.59E-2	2.05E-2
	$\tau_{max,root}$ [MPa]	399	352	358	322	333	314	347	393
	$\tau_{max,flank}$ [MPa]	267	223	198	192	191	199	227	245
EP-185-12.9-2-0.10-8-0.0	ε_{root}	9.24E-3	2.24E-2	1.87E-2	1.57E-2	1.46E-2	1.48E-2	1.65E-2	2.13E-2
	$\tau_{max,root}$ [MPa]	451	381	375	338	344	340	338	371
	$\tau_{max,flank}$ [MPa]	350	253	215	195	200	205	218	253
EP-185-12.1-2-0.10-8-0.0	ε_{root}	8.18E-3	2.01E-2	1.60E-2	1.45E-2	1.40E-3	1.51E-2	1.77E-2	2.37E-2
	$\tau_{max,root}$ [MPa]	393	351	333	312	316	328	330	398
	$\tau_{max,flank}$ [MPa]	263	214	198	200	185	189	214	284

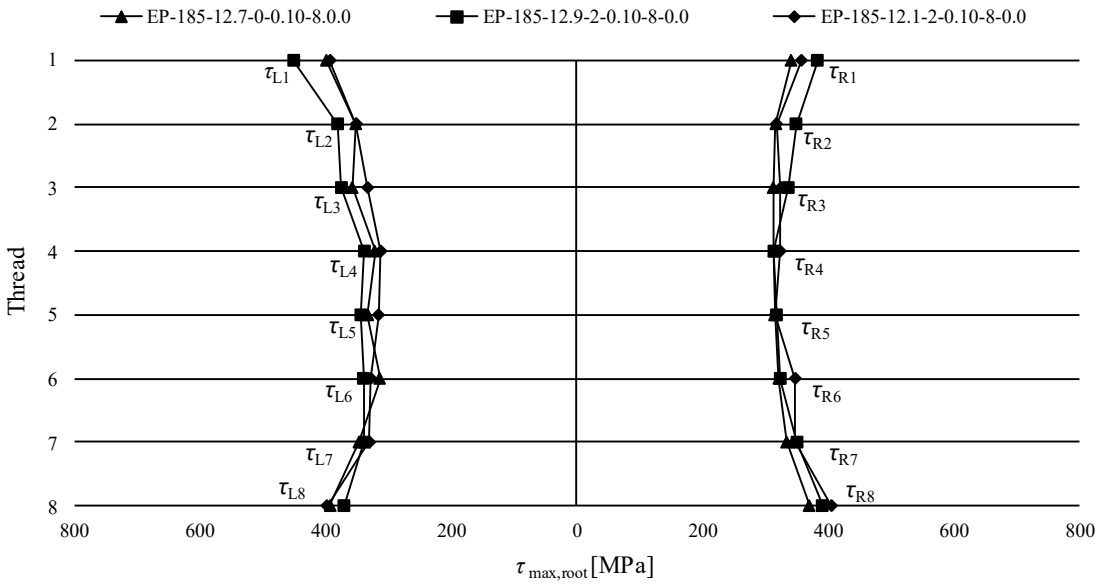

Figure 36. Maximum shear stress through the root of threads of the nut. Elastic-plastic material model. $F_L = F_R = 5$ kN, $t_1 = 0.917$ mm, $\mu = 0.1$, $F_S = 185$ kN.

4.5 Bold preload comparison

Strain values ε_{root} of the root of the ninth contacting thread on the right-hand side of the bolt (marked b_{R9} in figure 19) are compared with two different bolt preload values and one bolt load value that represents the bolt load under external load. The lowest bolt load values are corresponding with bolt preloads that are achieved with 500 N m and 700 N m tightening torque (Appendix I). Strain-life fatigue analysis is applied to the root of the bolt thread for estimation of how preload affects crack nucleation time (Appendix IV). Selected location b_{R9} has the highest maximum principal stress of threads of the bolt.

Table 18. Simulation parameters of two-dimensional FE-analysis of non-tapered bolt with elastic-plastic material model. Thickness parameter value t_1 varies depending on the bolt load F_S.

Simulation model	Force F_L [N]	Force F_R [N]	t_1 [mm]	Friction coefficient μ	Load eccentricity L_e [mm]
EP-132-12.7-0-0.10-8-1.0	4742	5258	1.283	0.10	1.0
EP-185-12.7-0-0.10-8-1.0	4742	5258	0.917	0.10	1.0
EP-300-12.7-0-0.15-8-1.0	4742	5258	0.564	0.10	1.0

Table 19. Strain values ε_{root} at the root of the ninth thread b_{R9} on the right-hand side of the bolt.

Simulation model	ε_{root} b_{R9}
EP-132-12.7-0-0.10-8-1.0	4.41E-3
EP-185-12.7-2-0.10-8-1.0	6.48E-3
EP-300-12.7-2-0.10-8-1.0	1.13E-2

4.6 Strain values of threads of the nut

Peak tensile strain values are extracted from the root of the last contacting thread n_{R8} for comparison.

Table 20. Strain values ε_{root} at root of the thread of eighth contacting thread n_{R8} on the right-hand side of the bolt.

Simulation model	ε_{root} n_{R8}
EP-132-12.7-0-0.10-8-1.0	3.56E-3
EP-185-12.7-2-0.10-8-1.0	5.54E-3
EP-300-12.7-2-0.10-8-1.0	1.70E-2

Both maximum strain and strain amplitude are larger on the thread of the nut side than on the bolt.

5 DISCUSSION

The effect of eccentric loading causes a high increase to a stress concentration factor of the first contacting thread but not to the last thread, which carries the second most load in compression-loaded bolt joint. If load eccentricity is high enough, the shank of the bolt may reach a tensile stress state subjecting the shank to fatigue damage as well as the first contacting thread is more likely to get damaged.

5.1 Findings of simulation results

The friction coefficient between threads has a large effect on achieved bolt preload, but it does not appear to be major a contributor to stress concentration levels at the root of the thread when bolt load values are the same. However, the friction coefficient between threads may play an important role in the fretting fatigue phenomenon of thread flanks.

Increased thread engagement length reduces stress concentration levels at the root of the thread and shear stress levels through thread flanks. Generally speaking, the thread engagement length with a tension-loaded bolt does not improve the fatigue strength after a certain point because fatigue damage usually occurs at the root of first contacting threads due to the combination of stress concentration factor and tensile stress state at the notch. With compression-loaded bolt, this same generalization does not apply if the root of the first contacting thread is at a compressive stress state which prevents the crack growth. Thus, further increased thread engagement length may be beneficial for the compression-loaded bolted joint. Fatigue failure is not expected to occur in the first thread, and increasing the thread engagement length reduces the shear stress levels across all the threads. Increasing the number of engaged threads from 6 to 8 reduced the maximum shear stress levels of first engaged threads by approximately 12%, and the total strain at the root of the first contacting thread was reduced by 19%.

Stress distribution of threads can be adjusted by tapering the threads. Tapering the first contacting threads of bolt reduced maximum shear stress levels of the first contacting thread of bolt by 21% and total strain at root of the thread by 25%. The maximum shear stress levels

of the corresponding thread of the nut side increased by 13%, and the total strain of root increased by 14%.

5.2 Crack nucleation comparison with different bolt preload values

Total strain values of the bolt at the root of the ninth thread on the right-hand side b_{R9} are determined with different bolt load values in chapter 4.5. These strain values are used to calculate the number of load cycles until crack nucleation by applying strain-life analysis. Peak to peak bolt load amplitude is between F_V…300 kN. Strain-life fatigue calculation is performed in Appendix IV.

Table 21. Amount of load cycles until crack nucleation with two different bolt preload values. Load varies between F_V…300 kN. Location b_{R9} of the bolt. Load eccentricity L_e = 1.0 mm.

F_V [kN]	N_f
132	36000
185	700000

Table 22. Amount of load cycles until crack nucleation with two different bolt preload values. Load varies between F_V…300 kN. Location n_{R8} of the nut. Load eccentricity L_e = 1.0 mm.

F_V [kN]	N_f
132	2771
185	4354

In this analysis, the bolt preload has a significant effect on crack initiation time. Loss of bolt preload increases the bolt load amplitude and accelerates the crack initiation. However, it is dependent on the type of bolted joint whether bolt load amplitude reduction is achieved by increasing the bolt preload. With the bolted joint diagram shown in figure 5, the bolt load amplitude reduction can be achieved by increasing the bolt preload. On the other hand, different type of bolted joint described in figure 7 does not benefit from the increased bolt preload similarly because the external load is added on top of bolt preload with bolt load multiplication. In this type of bolted joint, the static load capacity may be reduced if bolt preload is increased. Overloading of the bolt may cause the threads to deform, shear off or lead to loss of bolt preload.

6 CONCLUSIONS

The hypotheses of the study were to improve the fatigue strength of the compression-loaded bolt joint by changing the bolt preload and by modifying the thread geometry of the bolt.

Fatigue can occur in a structure that is under purely compressive external load because part geometry may cause local tensile- and shear stresses. Another possible cause of fatigue phenomenon in a compression-loaded bolted joint is residual stresses in part.

Reduction of bolt load amplitude by increased bolt preload is dependent on the bolt joint structure. Secondly, fatigue damage is not expected to occur in the shank section of the bolt if the bending stress component is not high enough to cause a tensile state to the shank in any part of the load cycle. However, increased bolt preload improves the fatigue strength of threads if the bolted joint structure is such that bolt load amplitude reduction is achieved. The location of the highest tensile stress state of compression-loaded bolt depends on load eccentricity and thread profile. With a standard thread profile, the location of the highest tensile stress is found from the root of the last contacting thread in both the bolt and the nut.

Based on two-dimensional finite element analysis results, it would be possible to improve the fatigue life of the bolt by adding a slight taper to threads so that the load is distributed more evenly between threads. On the other hand, it should be ensured that improving the fatigue strength of the bolt does not lead to reduced fatigue life of the nut.

This study has raised ideas about how the reliability of compression-loaded bolted joint could be improved by changes to the thread geometry, level of bolt preload, and structure of the bolted joint in terms of bolt load ratio and by minimizing the bending load that the bolt is subjected to.

REFERENCES

Airila, Ekman, Hautala, Kivioja, Kleimola, Martikka, Miettinen, Niemi, Ranta, Rinkinen, Salonen, Verho, Vilenius, Välimaa. 2010. Koneenosien suunnittelu. WSOYpro Oy Helsinki. 796 p.

Attia, H. Waterhouse, R. 1992. Standardization of Fretting Fatigue Test Methods and Equipment. American Society for Testing and Materials. Philadelphia. 16 p.

Brennan, F. 1992. Fatigue and Fracture Mechanics Analysis of Threaded Connections. Doctoral thesis. Department of Mechanical Engineering, University College London. London. 107 p.

Eurocode 3: Design of steel structures 2005. - Part 1-9: Fatigue. European Committee for Standardization. Brussels. 18 p.

Hills, D. 1994. Mechanics of Fretting Fatigue. Department of Engineering Science, University of Oxford. Oxford. 42 p.

Hobbs, J. 1998. Aspects of the Stress and Fatigue Performance of Threaded Connectors. Doctoral thesis. Department of Mechanical Engineering, University of Sheffield. Sheffield. 6 p.

Kim, W. Kawai, K. Koyama, D. Miyazaki, D. 2007. Fatigue strength and residual stress of groove-rolled products. Journal of Materials Processing Technology, 194. 46 p.

Matdat d.o.o. Detailed report, AISI 4140. Material ID 265. [Referred 24.5.2021]. Available: https://www.matdat.com/DAT-Search.aspx

Outinen, H. Salmi, T. 2004. Lujuusopin perusteet. Pressus Oy, Tampere. 464 p.

Richard G. Budynas, J. Keith Nisbett. 2011. Shigley's Mechanical Engineering Design. McGraw-Hill. New York. 1082 p.

Sagheer, A. 2013. Effect of head wear on rail underhead radius stresses and fracture under high axle load conditions. Doctoral thesis. Centre for Sustainable Infrastructure Faculty of Engineering and Industrial Sciences. Swinburne University of Technology. 48 p.

SAE J1099. 2002. Technical Report on Low Cycle Fatigue Properties, Ferrous and Non-Ferrous Materials. Society of Automotive Engineering. Warrendale. 26 p.

SFS 3099. 1974. Metallien väsytyskokeiden yleiset periaatteet. Metalliteollisuuden standardisointiyhdistys ry. Helsinki. Suomen standardisoimisliitto SFS ry. 10 p.

SFS-ISO 5408. 2010. Screw threads. Vocabulary. Metalliteollisuuden standardisointiyhdistys ry. Helsinki. Suomen standardisoimisliitto SFS ry. 19 p.

SFS-ISO 68-1. 2010. ISO general purpose screw threads. Basic profile. Part 1: Metric screw threads. Metalliteollisuuden standardisointiyhdistys ry. Helsinki. Suomen standardisoimisliitto SFS ry. 7 p.

Smith, J. 1942. The effect of range of stress on the fatigue strength of metals. University of Illinois bulletin. University of Illinois Urbana. Urbana 37 p.

Stephens, R. Fatemi, A. Fuchs, H. 2001. Metal Fatigue in Engineering. A Wiley-Interscience Publication. New York, 472 p.

Vingsbo, O. Söderberg, S. 1987. On Fretting Maps. Wear. International Conference on Wear of Materials. Houston. Pp. 131-142.

APPENDIX I

Bolt preload calculation

Bolt tightening torque M_A is calculated as per formula 6.

Table 23. Dimensions and friction coefficients of a bolt.

M_A	Bolt tightening torque	700 N m
μ_G	Friction coefficient of the thread	0.10
μ_K	Friction coefficient of bearing surface of the bolt	0.10
D_{km}	Average diameter of bearing surface of the bolt	38.9 mm
P	Thread pitch	3.175 mm
d_2	Pitch diameter of 1" UNC thread	23.2 mm

$$M_A = M_G + M_K = \frac{1}{2} F_M \left(1{,}155 \mu_G d_2 + \mu_K D_{km} + \frac{P}{\pi}\right)$$

Axial force during torquing F_M is equal with bolt preload F_V:

$$F_V = F_M = \frac{2M_A}{1{,}155 \mu_G d_2 + \mu_K D_{km} + \frac{P}{\pi}}$$

$$F_V = \frac{2 \cdot 700\ Nm}{1{,}155 \cdot 0.10 \cdot 23.2\ mm + 0.10 \cdot 38.9\ mm + \frac{3.18\ mm}{\pi}} = 185\ kN$$

The same formula is applied with bolt tightening torque of 500 N m:

$$F_V = \frac{2 \cdot 500\ Nm}{1{,}155 \cdot 0.10 \cdot 23.2\ mm + 0.10 \cdot 38.9\ mm + \frac{3.18\ mm}{\pi}} = 132\ kN$$

APPENDIX II

Buckling of the bolt

Table 24. Properties of the bolt joint.

C	End condition constant	0.25
E	Young's modulus	200 GPa
I	Second moment of area	10606 mm^4
L	Length of smooth section of shank	21.50 mm
d_1	Diameter of shank	21.56 mm

Second moment of area:

$$I = \frac{\pi {d_1}^4}{64} = \frac{\pi(21.56\ mm)^4}{64} = 10606\ mm^4$$

Buckling of the 1" UNC bolt is calculated by applying Euler's column formula:

$$P_{\mathrm{cr}} = \frac{C\pi^2 EI}{L^2} = \frac{0.25\pi^2 \cdot 200\ GPa \cdot 10606\ mm^4}{(21.56\ mm)^2} = 11323\ \mathrm{kN}$$

Load eccentricity and nominal stress of shank

External load eccentricity L_e that is used with two-dimensional finite element analysis is calculated as per formula 17. Two different external load value pairs are determined for 1 mm and 2 mm eccentric loading that are used with simulations.

Table 25. Distances and load values of two-dimensional FEA-simulation of a bolt with eccentric load of 1.0 mm.

L_1	Distance between bearing face center points	38.9 mm
F_R	External load on the right-hand side bearing face	5258 N
F_L	External load on the left-hand side bearing face	4742 N

$$L_e = \frac{L_1 F_R - L_1 F_L}{2F_R + 2F_L}$$

$$L_e = \frac{38.9\ mm \cdot 5258\ N - 38.9\ mm \cdot 4742\ N}{2 \cdot 5258\ N + 2 \cdot 4742\ N} = 1.0\ mm$$

Table 26. Distances and load values of two-dimensional FEA-simulation of a bolt with eccentric load of 2.00 mm.

L_1	Distance between bearing face center points	38.9 mm
F_R	External load on the right-hand side bearing face	5515 N
F_L	External load on the left-hand side bearing face	4485 N

Calculation of nominal stress σ_0 of shank with symmetric load condition:

Table 27. Force values, minor diameter, and thickness parameter of the bolt with symmetric load condition.

F_R	External load on the right-hand side bearing face	5000 N
F_L	External load on the left-hand side bearing face	5000 N
d_1	Minor diameter of the bolt	21.56 mm
t_1	Thickness parameter	0.917 mm

$$\sigma_0 = \frac{F_L + F_R}{d_1 t_1}$$

$$\sigma_0 = \frac{5000\ N + 5000\ N}{21.56\ mm\ \cdot 0.917\ mm} = 506\ MPa$$

Strain-life calculation

Crack nucleation time is calculated by applying local strain-life method with two different bolt preload values and single maximum bolt load value described in chapter 4.5.

Table 28. Material properties for AISI 4140 steel [Matdat d.o.o. 2021].

E	Young's modulus	211.4 GPa
K'	Cyclic strength coefficient	1367 MPa
n'	Cyclic strain hardening exponent	0.104
σ_f'	Fatigue strength coefficient	1454 MPa
ε_f'	Fatigue ductility coefficient	1.508
c	Fatigue ductility exponent	-0.716
b	Fatigue strength exponent	-0.075

Calculation of peak to peak strain amplitude $\Delta\varepsilon$:

$$\Delta\varepsilon = \varepsilon_{max} - \varepsilon_{min}$$

$$\Delta\varepsilon = 0.01136 - 0.00441 = 0.00695$$

Strain amplitude in with 500 N m tightening torque and 300 kN bolt load when external load is applied to the bolted connection:

$$\frac{\Delta\varepsilon}{2} = \frac{0.00695}{2} = 0.00348$$

Calculation of load cycles to crack nucleation N_f (Koneenosien suunnittelu, 2010):

$$\frac{\Delta\varepsilon}{2} = \frac{\sigma'_f}{E}(2N_f)^b + \varepsilon'_f(2N_f)^c$$

$$0.00348 = \frac{1454\ \text{MPa}}{211.4\ \text{GPa}}(2 \cdot 36000)^{-0.075} + 1.508(2 \cdot 36000)^{-0.716}$$

Value of 36000 for N_f is found by iterative method.

Same procedure is applied for the 185 kN bolt preload value.

Table 29. Strain- and load cycle calculation results with two different bolt preloads. Location b_{R9} of the bolt thread.

F_V [kN]	ε_{min}	ε_{max}	$\Delta\varepsilon$	N_f
132	0.00441	0.01136	0.00695	36000
185	0.00648	0.01136	0.00488	700000

Location n_{R8} of the nut:

$$0.00675 = \frac{1454\ \text{MPa}}{211.4\ \text{GPa}}(2 \cdot 2771)^{-0.075} + 1.508(2 \cdot 2771)^{-0.716}$$

Table 30. Strain- and load cycle calculation results with two different bolt preloads. Location n_{R8} of the nut thread.

F_V [kN]	ε_{min}	ε_{max}	$\Delta\varepsilon$	N_f
132	0.00356	0.01706	0.01350	2771
185	0.00554	0.01706	0.01152	4354